USDA
United States Department of Agriculture

The Dynamic General Vegetation Model MC1 Over the United States and Canada at a 5-Arc-Minute Resolution: Model Inputs and Outputs

Raymond J. Drapek, John B. Kim, and Ronald P. Neilson

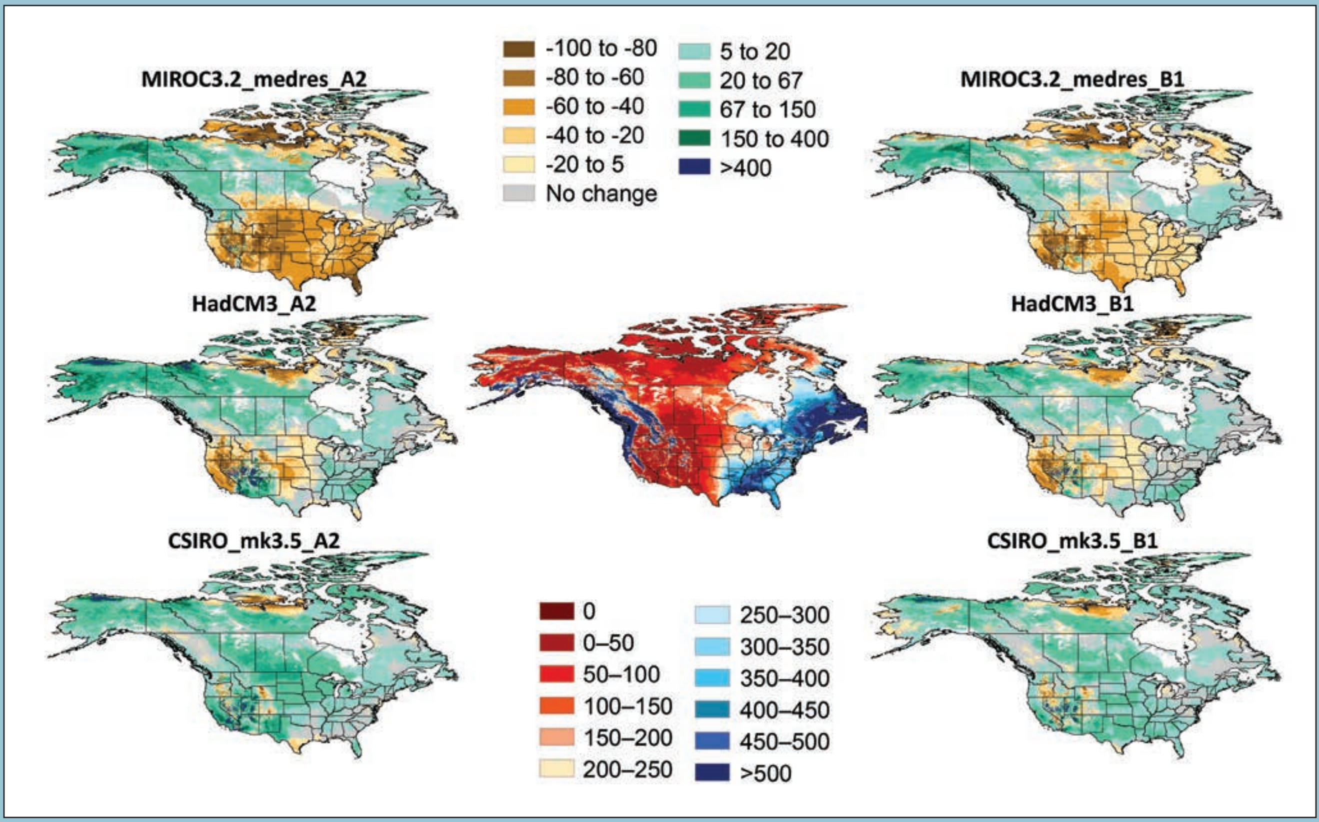

Forest Service
Pacific Northwest Research Station
General Technical Report PNW-GTR-904
November 2015

Authors

Raymond J. Drapek is a biologist and geographic information system specialist, and **John B. Kim** is a biological scientist, U.S. Department of Agriculture, Forest Service, Pacific Northwest Research Station, Forestry Sciences Laboratory, 3200 SW Jefferson Way, Corvallis, OR 97331-8550; **Ronald P. Neilson** is a professor (courtesy), Oregon State University, 1895 SW Whiteside Drive, Corvallis, OR 97333.

Abstract

Drapek, Raymond J.; Kim, John B.; Neilson, Ronald P. 2015. The Dynamic General Vegetation Model MC1 over the United States and Canada at a 5-arc-minute resolution: model inputs and outputs. Gen. Tech. Rep. PNW-GTR-904. Portland, OR: U.S. Department of Agriculture, Forest Service, Pacific Northwest Research Station. 57 p.

Land managers need to include climate change in their decisionmaking, but the climate models that project future climates operate at spatial scales that are too coarse to be of direct use. To create a dataset more useful to managers, soil and historical climate were assembled for the United States and Canada at a 5-arc-minute grid resolution. Nine CMIP3 future climate projections were downscaled to this grid and the MC1 dynamic global vegetation model was run over the historical and future climates. Climate variables included monthly mean temperature, precipitation, minimum temperature, maximum temperature, and vapor pressure. Soil data included soil depth as well as percentages of sand, clay, and rockiness for three soil depths. Output variables included carbon pools and fluxes, fire variables, potential vegetation classes, and various water cycle variables. Climate and soil inputs as well as MC1 outputs are available publicly.

Keywords: MC1, Dynamic Global Vegetation Model, climate change, carbon, fire, streamflow.

Summary

Land managers need to include climate change in their decisionmaking, but the climate models that project future climates operate at spatial scales that are too coarse to be of direct use. For this project, several alternative future climate scenarios were downscaled to a spatial scale that is more useful. Our goal for this project is to provide climate and soil inputs for a dynamic vegetation model and outputs from the model. A historical average climate dataset (1961–1990) was assembled to cover the United States (excluding Hawaii) and Canada at a 5-arc-minute grid resolution using 4-km data from the Parameter-Elevation Regressions on Independent Slopes Model (Daly et al. 2008) and data provided by Natural Resources Canada (McKenney et al. 2004, Price et al. 2004). Climate variables include monthly mean temperature, precipitation, minimum temperature, maximum temperature, and vapor pressure. Temporal monthly historical climate data for the years 1901–2000 were produced using an anomaly approach with the abovementioned average climate as a baseline and with climate anomalies coming out of TS 2.0 data provided by the Climatic Research Unit (Mitchell et al. 2004). Future climate was also assembled using an anomaly approach with the same baseline climate as was used for the temporal historical climate. Future scenarios are a 3 by 3 combination of three General Circulation Models (GCMs) and three greenhouse gas (GHG) emission scenarios from the Special Report on Emissions Scenarios (SRES) (Nakicenovic et al. 2000). The GCMs used are MIROC 3.2 medres (Hasumi and Emori 2004), HadCM3 (Johns et al. 2003), and CSIRO Mk3.5 (Gordon et al. 2010), identified in this report as MIROC, HadCM3, and CSIRO, respectively. The SRES scenarios are A2, A1B, and B1.

The soil data that were used include soil depth as well as percentages of sand, clay, and rockiness for three soil depths. Soil data were assembled from the Natural Resources Conservation Service State Soil Geographic (STATSGO) database (USDA NRCS 1994) and from the Canadian Soil Information System (MacDonald and Kloosterman 1984). The STATSGO data were gridded by Jeffrey S. Kern (Kern 1995).

The MC1 model can potentially output more than 900 annual or monthly variables. For this dataset, we included 25 annual variables including 2 variables describing biogeography, 2 variables describing fire, 2 leaf area index variables, 12 carbon stock variables, 4 carbon flux variables, and 3 hydrology variables.

MC1 outputs of several variables were compared against benchmark data for past years. The MC1 historical vegetation class map has a Kappa of 0.46 when compared with aggregated Küchler (1964) data. MC1 aboveground vegetation carbon correlates with the National Biomass and Carbon Dataset (Kellindorfer et al.

2012) with an R^2 of 0.46 and tends to be 2200 g m^{-2} higher. Comparisons of MC1 streamflow estimates versus three stream gages result in one stream gage from which MC1 values are consistently high, one from which MC1 values are low, and one from which MC1 values are low and high in roughly equal proportions. These comparisons yield R^2 values of 0.33, 0.49, and 0.62, respectively. MC1 fire return intervals are generally outside of the range estimated by Leenhouts (1998) for various potential vegetation types, with MC1 fires tending to be less frequent through much of the Eastern United States and more frequent through much of the West.

For 2071–2100, MC1 projects 33 to 51 percent of the land area changing in vegetation cover, with most of the changes happening in northern latitudes where large areas of tundra are replaced by forests. Increases in vegetation carbon and streamflow also are most pronounced in the far north. Biomass consumed by fire increases across much of the study domain for all nine future scenarios. For no location does a consistent decrease occur.

Contents

Introduction

In this report, we describe the production of a dataset that includes input for running the MC1 dynamic vegetation model (Daly et al. 2000) as well as some of the output coming from the model. This dataset covers the United States (excluding Hawaii) and Canada with a 5-arc-minute grid resolution (approximately 8 km per grid-cell side at mid latitudes). This dataset is an updated version of a 5-arc-minute dataset that previously had been distributed widely without publication. Included are descriptions of how soil and historical climate input data were assembled and how future climate data were downscaled from coarse-scale general circulation model (GCM) output. Results from the MC1 model are examined for broad patterns, including changes to vegetation type, vegetation biomass, fire return interval, biomass consumed by fire, and streamflow.

The current dataset is the first fully vetted and documented dataset for MC1 over North America at a 5-arc-minute grid resolution. Input and output files are available for general distribution. The MC1 code and parameters used are also available. The methods used to downscale the data are documented in this report.

For this project, we downscaled nine future climate projections. These are a combination of three GCMs and three greenhouse gas (GHG) scenarios from the Special Report on Emissions Scenarios (SRES) (Navkicenovic et al. 2000). Our choice of GCM/SRES scenarios was intended to span the range of projected GHG levels as well as the range of GCM responses to GHG levels. The three GCMs chosen were MIROC 3.2 medres (mild and wetter), HadCM3 (warm and dry), and CSIRO Mk3.5 (hot and dry). The three SRES scenarios chosen were A2, A1B, and B1. Since the initiation of this project, new climate model results for new emissions scenarios have become available through the Coupled Model Intercomparison Project Phase 5 (CMIP5). The new generation of climate change scenarios (e.g., Representative Concentration Pathways RCP 4.5 and RCP 8.5) in use for CMIP5 experiments were developed from SRES scenarios (IPCC WGII 2014, Moss et al. 2010, Riahi et al. 2011, Van Vuuren et al. 2011). The SRES scenarios A2 and B1 have comparable trajectories in terms of atmospheric carbon dioxide (CO_2) concentrations, radiative forcing, and mean surface temperatures, to RCP8.5 and RCP4.5 scenarios, respectively (IPCC WGII 2014, c.f. Rogelj et al. 2012, Van Vuuren et al. 2011). Therefore, we expect the general conclusions and broadly observed patterns to be comparable to MC1 simulations using RCP scenarios.

Inputs and outputs are available for download. Appendix 1 describes the geographic region, the graticule, and data-file formats. Appendix 2 describes how to obtain copies of the data.

Methods

The MC1 Model

The MC1 model is a dynamic vegetation model created to assess the impacts of global climate change on ecosystem structure and function at a wide range of spatial scales from landscape to global. The model consists of three linked modules (fig. 1): biogeography, biogeochemistry, and fire disturbance. The biogeographic module predicts the vegetation life forms (broadleaf/needleleaf, deciduous/evergreen, C3/C4) and classifies the vegetation into potential vegetation types (e.g., "Temperate Evergreen Needleleaf Forest"). The biogeochemical module simulates monthly carbon, nitrogen, and water dynamics. Aboveground and belowground processes are modeled in detail and include plant production, soil organic matter decomposition, and water and nutrient cycling. Parameterization of this module is based on the life-form composition of the ecosystems, which is updated annually by the biogeographic module. The fire module simulates the occurrence, behavior, and effects of severe fire. Allometric equations, keyed to the life-form composition supplied by the biogeographic module, are used to convert aboveground biomass to fuel classes. Fire effects (plant mortality and live and dead biomass consumption) are estimated as a function of simulated fire behavior (fire spread and fire line

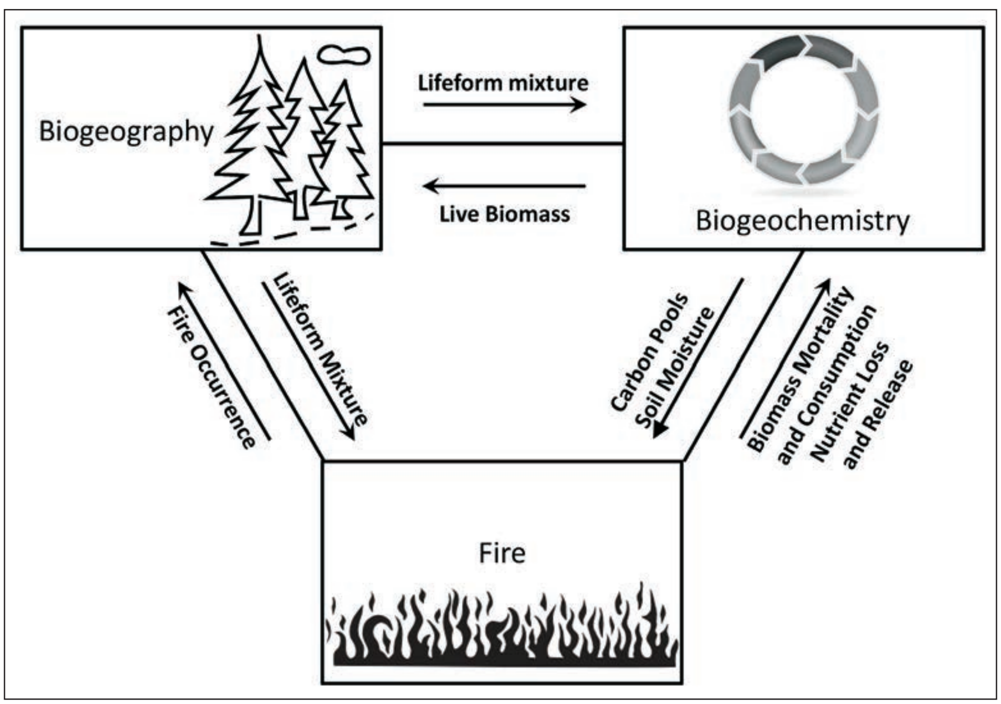

Figure 1—The three modules that the MC1 is composed of and the types of data that are passed among them.

intensity) and vegetation structure. Fire effects feed back to the biogeochemical module to adjust levels of various C and nutrient pools and alter vegetation structure. MC1 was originally introduced in Daly et al. (2000); a detailed description of the model can be found in Bachelet et al. (2001a). The MC1 model has been used for many purposes at several scales over many geographic domains (table 1).

In MC1, CO_2 levels affect plant production, potential evapotranspiration (PET), and carbon-to-nitrogen ratios (C:N). These are all adjusted using monotonically increasing and downward curved equations so that the adjustment is 1.0 at late-20th-century CO_2 levels and increases for higher CO_2 levels. The plant production, PET, and C:N adjustments rise to approximately 2.5, 2.2, and 1.9, respectively, for CO_2 concentrations of 800 ppm.

MC1 has undergone many revisions since its introduction. Revisions of MC1 source code are archived at the MC1 DGVM users website (https://sites.google.com/site/mc1dgvmusers/). For this project, we used the most recent version available at the inception of the project: a subbranch of Revision 165 called “LandCarbon.” It can be accessed from the lead author. This version derives from a Conservation Biology Institute project used to simulate carbon dynamics of the conterminous United States (http://databasin.org/groups/8d96fe463e514680a95c303acf532309). The most current LandCarbon project calibration at the time of the inception of this project was used. Of more than 900 possible annual and monthly output variables, we selected 25 key diagnostic annual variables to be shared. These variables cover carbon and water cycles, fire, and biogeography (table 2). Variables were chosen through interactions with people who used the output for various purposes and objectives. This list of variables has lengthened as the number of clients with different objectives has increased. The more variables that are included in the output, the slower the model runs on the computer, so this list also results from compromises between the time spent running the model and desired information quantity.

Simulation Protocol

MC1 execution was divided into four phases: EQ, spinup, historical, and future. Each phase was run in sequence and required its own dataset. First, in the EQ phase, the MAPSS model (Neilson 1995) was run over an average monthly climate for 1961–1990 to calculate the initial distribution of vegetation types. Then the biogeochemistry module ran for a maximum of 3,000 years over the same average monthly climate. The exact number of years the model is run in the biogeochemistry phase of the EQ depends on how long it takes for the resistant soil carbon pool to reach a stable state.

Table 1—Examples of published studies that made use of the MC1 model

Citation	Study	Geographic domain and scale
Bachelet et al. 2001b	MC1 results vs. MAPSS biogeography model	Conterminous United States at ½-degree grid
Bachelet et al. 2003	MC1 results vs. LPJ dynamic global vegetation model	Conterminous United States at ½-degree grid
Lenihan et al. 2003	Vegetation changes, carbon, and fire under two contrasting climate scenarios	California at 10-km grid
Bachelet et al. 2004	Carbon sequestration in six regions under future climate scenarios	Conterminous United States at ½-degree grid
Bachelet et al. 2005	Climate, fire, and ecosystem interactions in Alaska	Alaska at ½-degree grid
Gucinsky 2005	Climate change and natural resources management	Conterminous United States at ½-degree grid and California at 10-km grid
Galbraith et al. 2006	Biodiversity and adaptation under climate change	California at 10-km grid
Lenihan et al. 2006	Climate change assessment in California	California at 10-km grid
Bachelet et al. 2008	Different input dataset effects on vegetation distribution and carbon budget	Conterminous United States at ½-degree grid
Doppelt et al. 2008	Preparing for climate change in the Rogue River basin	Rogue River basin, Oregon, at 5 arc-minutes
Lenihan et al. 2008	Impact of fire management, carbon dioxide (CO_2) emissions, and plant CO_2 response on ecosystems under future climates	Conterminous United States at ½-degree grid
Kueppers et al. 2009	Feedbacks of terrestrial vegetation change to climate	California at 10-km grid
Gonzalez et al. 2010	What areas of the globe are vulnerable under climate change and what areas are potential refugia	Global at ½-degree grid
Koopman et al. 2010	Projected future climate and ecological conditions in San Luis Obispo County, California	San Luis Obispo County, California, at 5 arc-minutes
Halofsky et al. 2011	Climate change and vegetation management in the Olympic National Forest and Olympic National Park	Olympic Penninsula, Washington, at 30 arc-seconds
McLachlan et al. 2011	Prairie chicken conservation	Conterminous United States at ½ degree grid
Rogers et al. 2011	Impacts of climate change on fire regimes and carbon stocks	Western two-thirds of Oregon and Washington at 30 arc-seconds
Kerns et al. 2012	Climate-informed state and transition models	Central Oregon at 30 arc seconds
Halofsky et al. 2013	Climate-informed state and transition models	Central Oregon at 30 arc seconds

Table 2—Variables that were output from the MC1 model

Variable type	Variable name	Description	Units
Biogeography	nb_zone	Zone from global vegetation rules	None
	VTYPEyr	Potential vegetation type	None
Fire	PART_BURNyr	Fraction of cell burned	None
	bio_consume	Carbon in biomass consumed by fire	g C m^{-2}
Leaf Area Index (LAI)	max_tree	Maximum tree LAI	m^2 leaf m^{-2} ground
	max_grass	Maximum grass LAI	m^2 leaf m^{-2} ground
Carbon Stock	tslcx	Total soil carbon	g C m^{-2}
	C_SOMyr	Soil organic matter	g C m^{-2}
	C_ECOSYSyr	Total ecosystem carbon	g C m^{-2}
	max_rleavc	Maximum monthly tree leaf carbon	g C m^{-2}
	C_FORESTyr	Live tree carbon	g C m^{-2}
	treec	Maximum total tree carbon	g C m^{-2}
	aflivcx	Maximum aboveground live tree carbon	g C m^{-2}
	bflivcx	Maximum belowground live tree carbon	g C m^{-2}
	bdeadcx	Maximum belowground dead carbon (litter, not soil)	g C m^{-2}
	adeadcx	Maximum aboveground dead carbon	g C m^{-2}
	grassc	Maximum total grass carbon	g C m^{-2}
	C_VEGyr	Maximum annual total vegetation carbon	g C m^{-2}
Carbon Flux	nppx	Net primary production	g C m^{-2} yr^{-1}
	rspx	Heterotrophic respiration	g C m^{-2} yr^{-1}
	nepx	Net ecosystem production	g C m^{-2} yr^{-1}
	NBPyr	Net biome production	g C m^{-2} yr^{-1}
Water	AETyr	Actual evapotranspiration	mm H_2O yr^{-1}
	PETyr	Potential evaporation	mm H_2O yr^{-1}
	STREAMFLOWyr	Streamflow (= stormflow + baseflow + runoff)	mm H_2O yr^{-1}

In the spinup phase, MC1 ran for 2,000 years with detrended transient historical climate data. These data retain the seasonal and interannual variability observed in the historical data without the century-long trend. The detrended historical climate dataset was created by calculating an anomaly for each month relative to a 30-year moving average centered at that month. This anomaly was then added to the average 1901–1915 climate values. Detrended precipitation was cropped to ensure that no negative precipitation values resulted. The spinup phase established a seasonally and annually varying but stable fire regime.

In the third and fourth phases, the historical and future phases, respectively, MC1 was run with historical and future climate data to simulate historical and future responses of vegetation to climate conditions. The processes we used to create appropriate climate datasets for all the phases are described in detail below.

Model Inputs

Soil

MC1 soil data requirements include 11 variables: percentages of sand, clay, and rock for three soil depths; overall bulk density; and mineral depth. The three soil depths used by MC1 were surface (0 to 50 cm), intermediate (50 to 150 cm), and deep (>150 cm). Because the soil dataset for this project covered a large area over two countries, soil datasets from three sources had to be combined.

Gridded soil data for Alaska were derived from STATSGO (USDA NRCS 1979) by Jeff Kern using approaches described in Kern (1995). Kern's data are gridded at a 1-km grid resolution and projected using an Albers conical equal area projection. Kern's gridded Alaska data contain the 11 variables that we required for this project. We converted these data to our 5-arc-minute geographic coordinate system. This was done using the "Project Raster" tool in ArcMap 10.0 using the "nearest" resampling technique.

Soil data for Canada came from the Canada Soil Information System (CanSIS) (MacDonald and Kloosterman 1984). To create our 11-variable gridded data, we had to combine data from many files. The CanSIS data came as multiple ASCII grids, one for each combination of mineral soil component, variable (e.g., percentage of sand), and vertical soil section. For each soil depth layer, we obtained data from each of one to four mineral components. These values were then used to calculate a weighted average by using the area per mineral component to do the weighting. Once the weighting was completed, we modified values to account for differences in the mineral depths of our source dataset versus our target. The CanSIS data were provided at depths of 0 to 50, 50 to 100, and 100 to 150 cm, whereas MC1 requires soil data in layers 0 to 50, 50 to 150, and >150 cm. Weighted averaging by depth was done using depth overlaps of the target and source datasets as weighting factors.

The CanSIS data came as 10-km gridded data in a NAD83 Canada Atlas Lambert projection. Once we had assembled grids for our 11 variables as described above, we needed to convert the data from the 10-km projected coordinate system to our 5-arc-minute geographic coordinate system. This was done using the "Project Raster" tool in ArcMap 10.0 using the "nearest" resampling technique.

Gridded soil data for the conterminous United States were derived from STATSGO (USDA NRCS 1979) by Jeff Kern using approaches described in Kern

(1995). Kern's data for the conterminous United States are gridded over a geographic coordinate system at a 30-arc-second grid resolution. Kern's gridded data contain the 11 variables that we required for this project. We converted these data to our 5-arc-minute geographic coordinate system using the "Project Raster" tool in ArcMap 10.0 using the "majority" resampling technique.

A challenge in creating the soil data was that the source datasets had "no soil" values for locations currently covered by either ice sheets or peatlands. The distinction between peat and ice was not coded in the source data. If all runs of the MC1 model were to be done in current times, it would be appropriate to simply mask out those grid cells. But for runs of the model under future scenarios, we had to consider the possibility that ice fields would melt and peatlands would dry up. We decided that with the current version of MC1 (and for the next few foreseeable versions) we would not have the ability to simulate peatlands, but we could run the model over melted ice fields. Therefore, the two cell types had to be distinguished, the peatlands had to be masked out, and some defendable value for the soil attributes had to be found for ice-field locations. To that end, we used the Harmonized World Soil Database (HWSD) (Nachtergaele et al. 2009) both to distinguish peatlands from ice fields and to fill in soil attributes for ice field locations. Using topsoil organic carbon values from the HWSD data, we identified grid cells that were in the top 10th percentile and used them to create a peatland mask. Grid-cell sizes for this mask were very coarse relative to our CanSIS and STATSGO sources, and there was not always a complete match-up in values. For example, there were CanSIS grid cells that were too far south and low in elevation to be ice fields, so they had to be peatlands, but were not tagged as such in the HWSD mask. For this reason, we could not use the peatland mask directly but instead used it to conceptually assemble some rules with which we could make the distinction between peatlands and ice fields over our 5-arc-minute grid. Those rules are:

1. All Alaska peat/ice grid cells are ice.
2. All peat/ice grid cells for states, provinces, and territories east of the Rocky Mountains are peat, with an exception of the territory of Nunavut.
3. In Nunavut, all peat/ice grid cells on Victoria Island, the Queen Elizabeth Islands, and Baffin Island are ice; otherwise they are peat lands.
4. All peat/ice grid cells in the Western States of the conterminous United States (Rocky Mountains and westward) are lakes (e.g., Great Salt Lake) and should be removed from the land mask. (For this rule we also consulted standard land cover maps.)
5. All peat/ice grid cells in British Columbia east of the Rocky Mountains are peatlands, and all to the west are ice.

6. All peat/ice grid cells in the interior Yukon Territory are peatlands, and all in the coastal mountains are ice.

Note that these rules were not used to describe all locations within these regions. For example, we acknowledge that there are peatlands in Alaska, but at the 5-arc-minute resolution these rules worked reasonably well. Because the HWSD data are relatively coarse, the soil values have rectangular geographic patterns in the ice-field grid cells, but we concluded that this artifact was preferable to "no data" or infilling by extrapolating from surrounding grid cells. The geographic patterns in soil bulk density values stemming from the HWSD data can be seen in the Brooks Range in northern Alaska (fig. 2). The white grid cells seen in the interior Canadian provinces were excluded from simulation. These masked cells included both large lakes and peatlands.

Soil attributes in CanSis for Canada differ from those in STATSGO for the United States. Soil bulk density values in Canada were systematically higher than those in the United States (fig. 2). The difference is most apparent at the southern border of British Columbia. The direct effects of these systematic differences are observed in MC1 outputs. A search of the literature has revealed no comparative studies of these soil datasets, and it was beyond the scope of this project to investigate and address the systematic differences in attributes of the two soil datasets.

EQ, Spinup, and Historical Climate

As was noted in the "Simulation Protocol" section of this report, MC1 execution is divided into four phases: EQ, spinup, historical, and future. However, it is easiest to describe the climate datasets upon which these phases are run in a different order. For example, although the spinup data precede historical in the flow of MC1 execution, the spinup dataset itself is derived from the historical dataset. Therefore, the description of these datasets and their derivation will be done in a different order from that which occurs in an MC1 model run. Also, to describe how our historical climate dataset was assembled, we need to make the distinction between a transient and a baseline climate. For our purposes, a transient climate is a monthly gridded climate that changes from year to year, e.g., a 1,200-month dataset that covers all the months for the years 1901–2000. A "baseline" climate is a 12-month average for some set of years, e.g., the average climate for 1961–1990. From our sources we did not have a transient historical climate at the desired grid resolution, but we had baseline climates (1961–1990) for several regions across Canada and the United States at the desired grid resolution, and we had transient global climate data for the years 1901–2000 at a coarser grid resolution. Transient climate was provided by the Climatic Research Unit (CRU TS 2.0) (Mitchell et al. 2004).

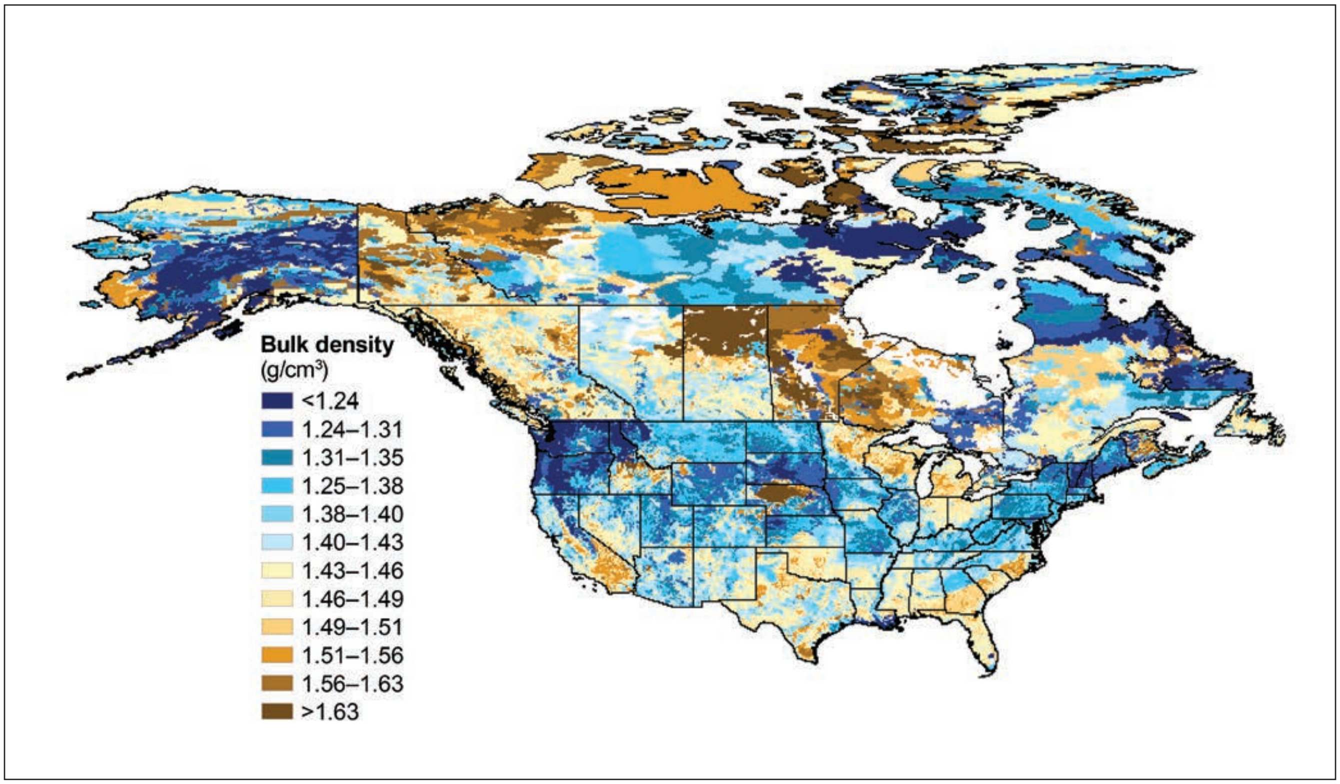

Figure 2—Assembled map of bulk density (grams per cubic meter). Canada grids of the map are derived from the Canada Soil Information System, and grids within the United States are derived from the State Soil Geographic dataset. A few grid cells that are currently ice-covered were derived from the Harmonized World Soil Database.

All of our climate data are ultimately derived from the 1961–1990 baseline climates. The baseline climate was created by integrating data from multiple sources (table 3). The Canadian Forest Service provided data for the entire study domain, but gridded using ANUSPLIN (Price et al. 2004). ANUSPLIN is a good approach for relatively flat terrain, but regions having significant terrain features, coastal effects, rain shadows, or cold air drainages and inversions are better handled by a system such as [Parameter-Elevation Regressions on Independent Slopes Model] PRISM (Daly 2006, 2008). For consistency, we would have used PRISM data for the entire dataset, but we did not have access to PRISM data for eastern Canada. For this project, PRISM data were used for all other portions of the domain (western Canada, Alaska, and the conterminous United States).

The Canadian Forest Service data came divided into regions that needed to be merged: Yukon and Northwest Territories, Nunavut, British Columbia, Prairie Provinces, Ontario, and the Quebec/Newfoundland and Labrador/Maritime provinces. The PRISM data files all came as 2.5-arc-minute grids and were regridded to the 5-arc-minute grid. The regridded data were a weighted average of input grid values, where the weighting was based on the area of overlap between the 2.5-arc-minute and the 5-arc-minute grid cells. Once all the data sources were at the

Table 3—Sources of gridded average historical climate (1961–1990)

	URL	Contact	Approach to gridding	Agency	Grid size
Alaska	http://www.climatesource.com	Chris Daly	PRISM	Climate Source	2.5 arc minute
Canada east of the Rocky Mountains	ftp://ftp.nofc.cfs.nrcan.gc.ca	David Price	ANUSPLIN	Natural Resources Canada, Canadian Forest Service	5 arc minute
Canada west of the Rocky Mountains	http://www.climatesource.com	Chris Daly	PRISM	Climate Source	2.5 arc minute
Continental United States	http://www.prism.oregonstate.edu	Chris Daly	PRISM	Oregon Climate Service	2.5 arc minute

5-arc-minute resolution grid, they were assembled into a single 12-month average (1961–1990) file. This 1961–1990 baseline climate was used for the "EQ" phase of the MC1 run.

Creation of a vapor pressure baseline climate was complicated by the fact that no water vapor data were available for Alaska and western Canada for the PRISM baseline climate. Therefore, vapor pressure values for these regions were calculated by interpolating CRU-based relative humidity (RH). To calculate RH from the CRU data, saturated vapor pressure at Tmean was calculated using equation 1 (Waring and Running 1998).

$$Satvp = 0.61078 \times \exp[(17.269 \times T)/(237 + T)], \tag{1}$$

where

Satvp = saturated vapor pressure (kilopascals) and

T = temperature (degrees Celsius).

Then we divided monthly vapor pressure by saturated vapor pressure to obtain RH. We then interpolated RH from the 0.5° CRU grid to the target 5-arc-minute grid using a bilinear interpolation. At the 5-arc-minute scale, mean saturated vapor pressure was calculated from mean temperature using equation 1. We then multiplied saturated vapor pressure by RH to produce the 5-arc-minute vapor pressure dataset.

To generate our transient historical data, we used the anomaly or "delta" method (Fowler et al. 2007) and downscaled the 0.5° climate date from the CRU TS 2.0 (Mitchell et al. 2004). This same anomaly approach was subsequently used to downscale GCM future climates. To implement the anomaly method, first we calculated anomalies of the CRU data to the baseline period 1961–1990 by taking the difference or a ratio of the climate value for each month versus the average for that month over the baseline set of years. The baseline climate used at this point is calculated from CRU climate. For the anomaly approach, the coarse grid anomalies are always generated from the coarse grid source relative to a baseline from the same source. Difference anomalies were used for temperature, and ratios were used for precipitation and vapor pressure. Second, we used bilinear interpolation to transform each anomaly grid to a 5-arc-minute resolution. A bilinear interpolation is an extension of linear interpolations to a 2D grid. A linear interpolation is performed first in one direction and then again in the other direction. Finally, we added or multiplied the interpolated anomalies to the gridded observed baseline climate. This is a fine-grid baseline and is different from the coarse-grid baseline that was used to create the anomalies in the first place. The results are monthly climate values that encapsulate long-term temporal trends from the transient (CRU) data and fine-scale spatial climate patterns from the baseline climate data. These are the data that are used in the “historical” phase of an MC1 run.

For the spinup phase of the model, we need a trend-free climate that varies from year to year, retains the variability found in the observed historical climate, and has average values that correspond with the climate at the start of the historical period. As was noted in “Simulation Protocol,” this phase of the model is used to build up aboveground carbon and fuel levels and establish dynamic fire events. The spinup data are derived from the transient historical data and are of the same length temporally but generally are run over many more years, so that for an MC1 run, the spinup climate data are cycled through many times. Unlike the historical or future data, no month in this dataset represesents any particular month in real time.

To create the spinup climate data, historical data were detrended by creating a time series of anomalies. These are 31-year running anomalies and are different from the anomalies used to downscale the CRU historical climate. For each month of the spinup climate, we started with the transient historical value for that month. An anomaly was calculated as the difference between that month’s climate value and the average for that month for the 31 years centered at that month. For months within 15 years of the start or the end of the historical data, the average was based on whatever proportion of the 31-year span was available. For our 1,200-month transient historical climate, we produced 1,200 monthly anomalies. These were added to a baseline climate based on the first 15 years of the historical data (1901–1915). The purpose for this step was to have the spinup transition smoothly into the historical data.

Future Climate

General Circulation Model outputs for future climate have relatively coarse resolution. Those used for this project had resolutions ranging from 1.85 to 3.75 degrees.

The data needed to be spatially downscaled to our 5-arc-minute grid. We used the same anomaly method to downscale the future climate that we used to downscale the CRU historical climate. This approach is described above. As was done with CRU, difference anomalies were used for temperature, and ratio anomalies were used for precipitation and vapor pressure.

The ratio anomalies used for precipitation posed some additional problems. There were some cases in which a GCM simulated zero precipitation for the 1961–1990 baseline period, which prohibited the calculation of the rainfall anomaly values. To fix this problem, all simulated average 1961–1990 precipitation values of zero were converted to the smallest nonzero value being produced by that GCM. A second problem was that some ratio anomalies were extremely large when the denominator values were very low, producing precipitation values in the final downscaled data that were well outside of what could reasonably be expected. Because of this, ratio anomalies were capped at a value of 5.0. This cap was chosen because it still represents a very large increase but is rarely exceeded. It was implemented over less than 1 percent of all the grid cell/months.

With the exception of HadCM3, data for all scenarios were obtained from the World Climate Research Program CMIP3 multimodel database website (https://esg.llnl.gov:8443/home/publicHomePage.do). NetCDF files were downloaded for the GCMs miroc_3_2_medres and csiro_mk3_5. Scenarios selected were sresa2, sresa1b, and sresb1. Data were also collected for the 20c3m (20th century) experiment. Variables obtained included huss (surface specific humidity), pr (surface precipitation), ps (surface air pressure), tas (surface air temperature), tasmax (surface average maximum temperature per month), and tasmin (surface average minimum temperature per month).

HadCM3 results were not available at the WCRP CMIP3 website, but instead had to be obtained from the British Atmospheric Data Centre (BADC), http://badc.nerc.ac.uk/home/index.html. BADC uses nonintuitive five-letter codes to designate different climate datasets. We selected aaxzl for historical data, aaxzi for A2 data, acfxd for A1B, and acfxc for B1. The data are in a proprietary format called Post Processing Format (PP). We used the program Convsh provided by BADC to convert the PP files to NetCDF.

HadCM3 data were daily values. We aggregated them to monthly values for input into MC1. The monthly value for temperature was calculated as an average of the daily values. HadCM3 data included RH but not vapor pressure. To calculate vapor pressure from RH, we first calculated saturated vapor pressure for the daily mean temperatures by using equation 1. We then multiplied saturated vapor pressure by RH. These daily vapor pressure values were then averaged for each month. Monthly precipitation was calculated by summing the daily values.

Vapor pressure (vpr) values were also not directly provided for the CSIRO and MIROC GCMs. However, surface-specific humidity (huss) and surface air pressure (ps) were available for all three SRES scenarios of MIROC 3.2 medres and for two out of the three scenarios for CSIRO Mk3.5 (A2 and B1). To convert from huss and ps to vpr the following equation was derived from the ideal gas law:

$$vpr = ((ps/(R x Tmean)) / ((Є/huss) + 1) \times R \times Tmean,$$

where

vpr = vapor pressure (pascals),

ps = surface air pressure (pascals),

Tmean = mean monthly temperature (degrees Celsius),

huss = specific humidity (kg/kg),

R = universal gas constant, 8318.97862 (liter-Pascal/K), and

Є = the ratio of the molecular weight of water vapor to dry air = 0.622.

Once monthly vpr values were obtained, we downscaled them by using the anomaly method described above. The method we used to obtain vapor pressure for the A1B scenario for CSIRO Mk3.5 is described in the next section.

Bias and Error Correction and Gap Filling

For both historical and future climate data, some variables or scenarios presented additional challenges that required us to modify our approach to producing the data. This section goes through some of those exceptions and describes the methods we used to respond to them.

Producing future Tmin and Tmax data proved more problematic than producing Tmean data. Because differences between the three variables (Tmin, Tmax, and Tmean) were often very small, small errors (e.g., rounding errors) often resulted in reversals of the proper order when we used the anomaly method for all three variables (fig. 3). To correct this problem, future Tmean values were produced first using the anomaly method. Tmin/Tmax values were then calculated based on the mean diurnal temperature ranges (Tmin – Tmean and Tmax – Tmean) at the original GCM resolution. The temperature ranges were then downscaled to the 5-arc-minute resolution and added/subtracted to/from the Tmean to create Tmax and Tmin values.

Using the original diurnal temperature ranges from GCM data introduced a new problem, resulting from the fact that the GCMs frequently had diurnal temperature ranges different from our historical data. If this difference was not taken into account, then the Tmin or Tmax data would often suddenly increase or decrease at the transition from historical to future depending on the size of the GCM average diurnal temperature range relative to the historical. For example, in the grid

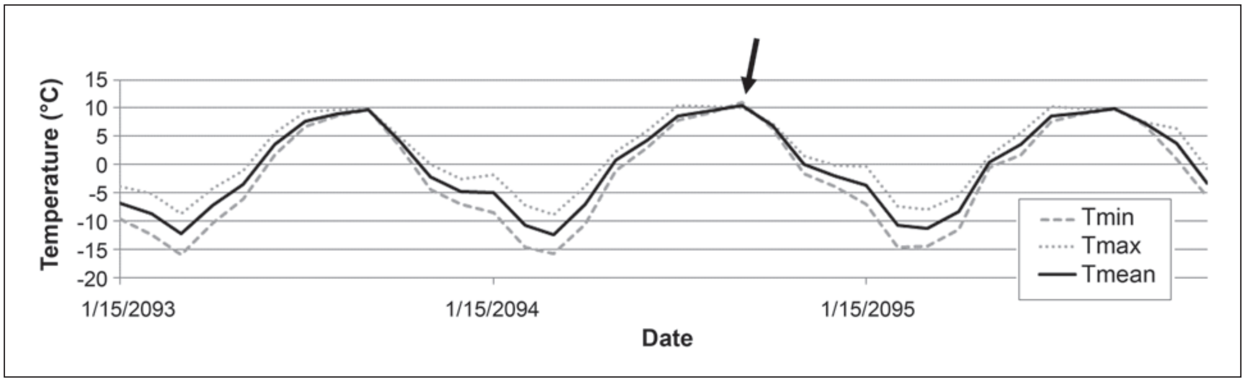

Figure 3—A demonstration of the problem with using the standard anomaly approach for Tmin, Tmean, and Tmax. In this graph tmin, tmean, and tmax values for a single grid cell are plotted over 3 years. In this case, all three climate variables were calculated by using the standard anomaly approach. Arrow indicates where the correct order of these variables gets reversed (i.e., Tmin > Tmean > Tmax).

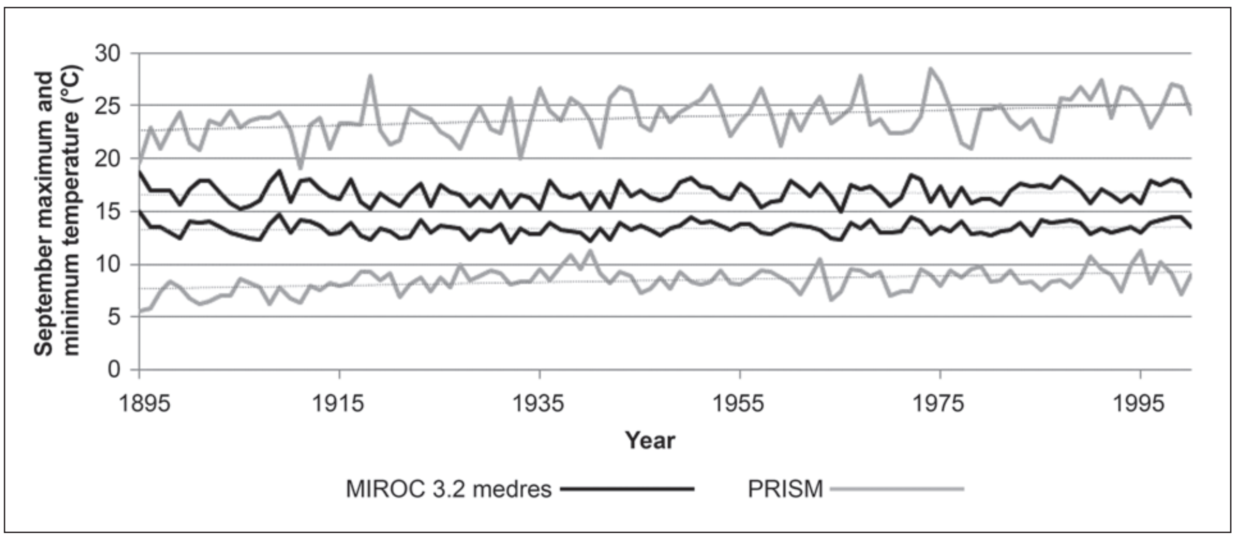

Figure 4—A demonstration of general circulation model (GCM) bias relative to PRISM climate. This is the plot of September Tmin and Tmax values for the grid cells enclosing Corvallis, Oregon. Gray lines are those from the PRISM dataset (based on interpolated weather station data). Grid-cells for this are 5-arc-minutes. Black lines are values simulated by the MIROC 3.2 medres GCM. These grid cells are approximately 2.8°.

cell containing Corvallis, Oregon (fig. 4), the diurnal temperature range based on MIROC 3.2 medres data is about 15° while the range for the PRISM data is generally less than 5 °C. The grid-cell sizes are different between MIROC 3.2 medres and PRISM, but even after you interpolate the GCM values to the finer grid, significant differences exist. Because of this, a bias correction had to be applied to the interpolated diurnal temperature ranges. To make this bias adjustment we took the following steps (Tmax example):

1. Calculate (Tmax – Tmean) for the GCM for each month over the historical period (1901–2000).

2. Calculate (Tmax – Tmean) for the historical data for each month over the historical period (1901–2000).
3. Spatially interpolate the (Tmax – Tmean) values from the GCM to the 5-arc-minute grid (simple bilinear interpolation).
4. For each grid cell and for each month in the year, get the average (Tmax – Tmean) values for both the historical and for the interpolated GCM data.
5. Subtract the historical average (Tmax – Tmean) value from the average GCM value to get the average bias of the GCM relative to the historical data.
6. When calculating future Tmax values, add the future interpolated GCM (Tmax – Tmean) values to the already downscaled future Tmean values, and then add the bias for each month.

Vapor pressure data were unavailable for Alaska and western Canada for PRISM baseline climate. Vapor pressure values for these regions were calculated by interpolating CRU-based RH. Saturated vpr at Tmean was calculated by using equation 1. We then divided monthly vpr by saturated vpr to obtain RH. We interpolated RH from the 0.5° CRU grid to the target 5-arc-minute grid by using a bilinear interpolation. At the 5-arc-minute scale, mean saturated vpr was calculated by using equation 1 because temperature data were available. They were then multiplied by the relative humidity values to produce the 5-arc-minute vpr dataset.

As for all the other climate variables, transient historical vpr data were created by downscaling from CRU-based anomalies. Relative humidity anomalies were used to calculate vpr. For each month CRU-based RH, values were calculated by using equation 1. The RH anomalies were calculated as ratios of each month's RH divided by the monthly baseline (1961–1990). Anomalies were interpolated to the 5-arc-minute grid by using bilinear interpolation. For the 5-arc-minute grid, monthly Tmeans were used to calculate saturated vpr. These were divided from the 5-arc-minute vpr values to produce RH values. These were multiplied by the interpolated RH anomalies to produce adjusted RH values, which were multiplied with the 5-arc-minute saturated vpr values to produce historical vpr values.

The CRU TS 2.0 vpr data had periods of time during which the seasonal pattern repeated for several years. These repetitive data segments caused problems for MC1, so these segments were replaced with new vpr values. The repetitive years were defined as any year in which the average of the 12 monthly vpr values was the same as in adjacent years. New vpr values were calculated from saturated vpr (satvp) at Tmin by using equation 1. The new vpr, values were further adjusted by the ratio of air pressure relative to sea level air pressure as suggested by Price et al. (2004). Air pressure was calculated as $P(z) = P(0) \times [(1.0 - 0.0065z/293.0)^{5.26}]$

where
P = the atmospheric pressure at a given elevation (pascals) and
z = elevation (meters).

Finally, an adjustment factor (AF) was applied to the new vpr values to ensure smooth transitions between the original vpr and the new vpr values. To create the AF, the new vpr values were created for all months, even when the original vpr data appeared valid. During time periods when the original data appeared valid, we calculated AF as the average difference between the original and the new vpr values. The AFs were then added to the new vpr values to align them with the original data (fig. 5).

The CMIP3 portal lacked any kind of water vapor data for the CSIRO Mk3.5 GCM when run over the A1B emission scenario. For this scenario, we calculated vpr by using the assumption that average RH values for the baseline period (1961–1990) also applied to the future. We calculated future vpr values for this scenario as follows:

1. For each month in the year and for each grid cell, we calculated the average RH for the years 1961–1990 from the historical dataset.

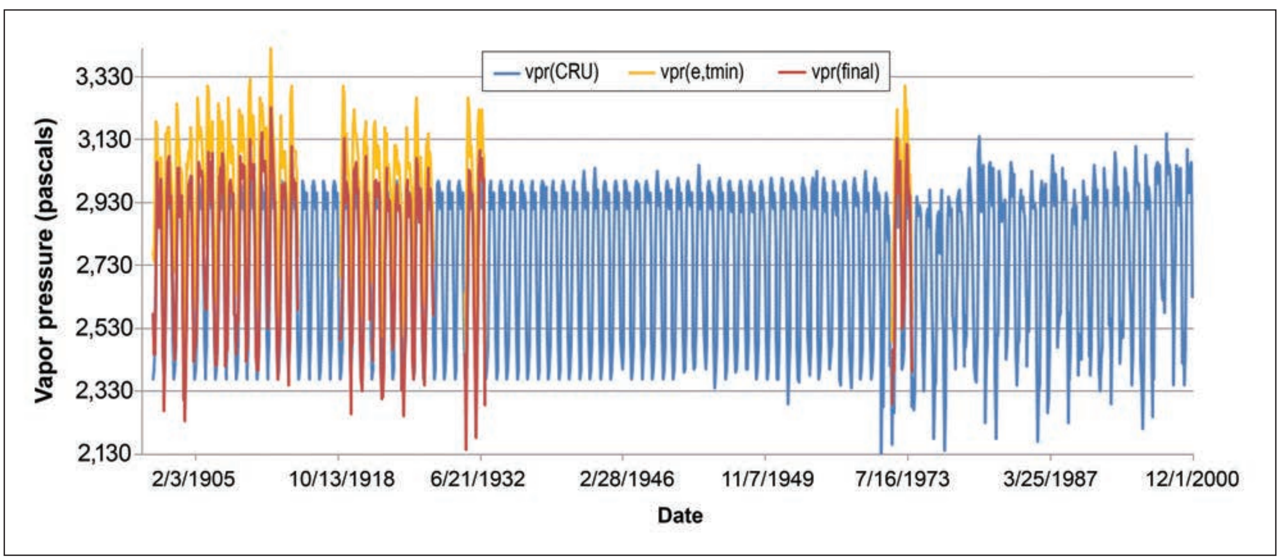

Figure 5—Example of removing unchanging vapor pressure (vpr) values from the Climate Research Unit (CRU) TS 2.0 data for a single grid cell. All years for which the average of the vpr values across all 12 months of that year equaled the average of an adjacent year were labeled "unchanging." Adjustments were only made for months within unchanging years. The blue line plots the original vpr values from CRU. Yellow lines represent vpr values calculated from saturated vpr at Tmin and adjusted for air pressure as described in Price et al. (2004). These vpr values were calculated for all months, even for those months for which no adjustment was needed. From the years where no adjustment was needed, the average of the difference between the calculated vpr and the CRU-based vpr values was calculated separately for each month of the year. This average difference was then used as an adjuster for those months where the surrogate was needed. The red line shows the adjusted vpr values.

2. For each future month, we calculated the saturated vpr for Tmean by using equation 1.
3. For each future month, we calculated vpr as the average historical RH for that month in the year multiplied by the saturated vpr for that month.

We tested this approach for scenarios where specific humidity (huss) data were available and found excellent agreement between the RH-based vpr values and the huss-based vpr values (fig. 6a). For CSIRO-A2, the RH-based vpr had a bias of 30.6 pascals at year 2001, increasing to about 60 pascals by year 2100 (fig. 6b). This was the largest bias observed for the three scenarios examined (MIROC B1, CSIRO A2, and CSIRO B1).

Quality Control

All climate data were checked three ways. First, the largest and smallest values in each data file were checked to make sure that all values were within a reasonable range as determined by our experience with previous historical datasets. Historical values could be exceeded, but values an order of magnitude or more outside the historical range were assumed to be problematic. Second, a time-series of average monthly values across the continent was plotted to assure that there were no spurious spikes and that reasonable temporal patterns were followed. For example, for these northern latitude locations, we expected to see summer temperatures that were higher than winter. Third, a map of average values was created for a range of years (1961–1990 for historical and 2070–2099 for future). The map was visually inspected to ensure that spatial patterns were reasonable. For example, we visually confirmed that temperatures were generally lower at higher latitudes and elevations. Additionally, for a subset of variables and scenarios, downscaled future climate anomaly maps were visually compared with climate anomaly maps produced from the GCMs at the original resolution.

Results

Climate

Temperatures increase everywhere in the study domain under all three emissions scenarios and for all three GCMs from the historical period (1961–1990) to the end of the century (2070–2099), with the greatest increases happening in the far north (fig. 7). The A2 emissions scenarios produce the most warming, and the B1 scenarios produce the least. The MIROC GCM produces the most warming, with average annual temperature increases across the continent rising to close to 9 °C by the end of the 21st century for the A2 emissions scenario (fig. 8). The HadCM3 and CSIRO

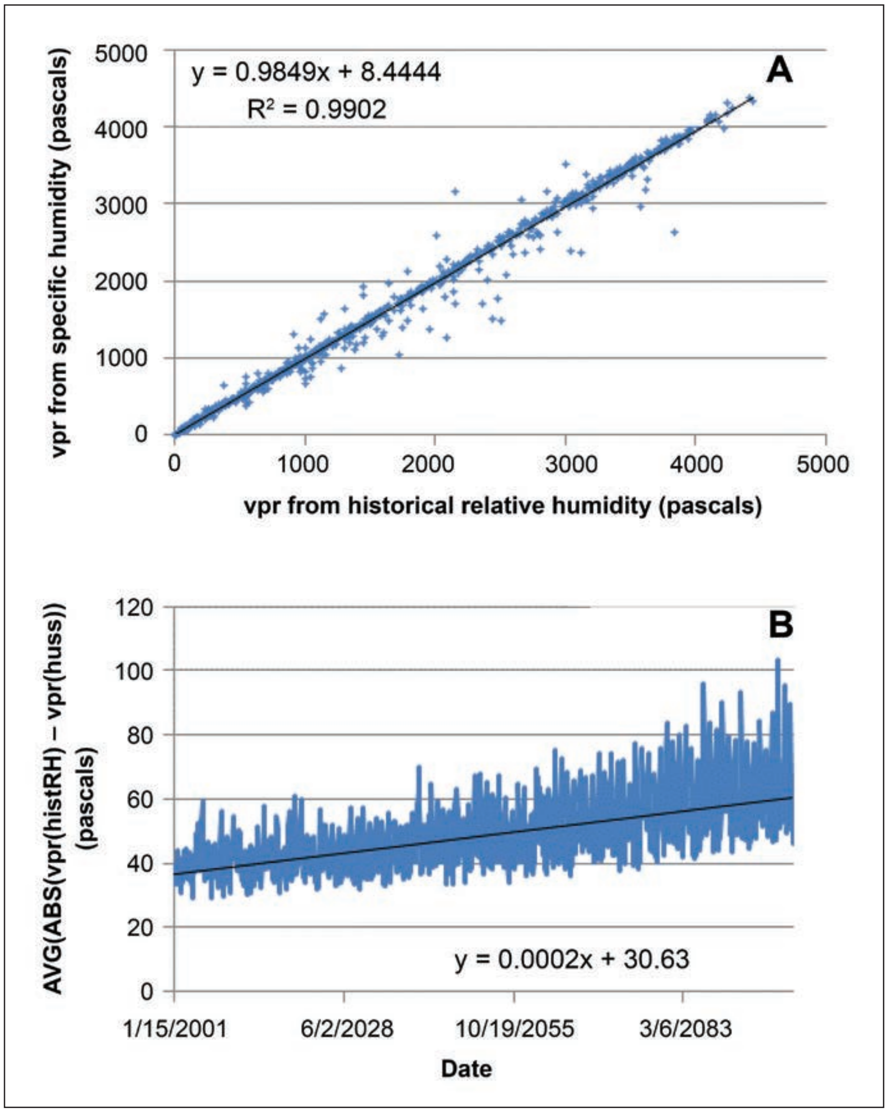

Figure 6—Vapor pressure (vpr) values calculated for the CSIRO Mk3.5 SRES A2 scenario by assuming that average relative humidity (RH) values for the baseline period (1961–1990) also apply to the future, versus vpr levels calculated from surface specific humidity (huss) data. The purpose of this comparison is to show how well the average RH approach approximates future surface atmospheric water vapor when no data are provided by the general circulation model. Figure 6a shows a scatterplot of all grid cell/ months across the years 2001–2100 of vpr values calculated with the two alternative methods. Figure 6b shows the average value for the difference between the RH-based vpr versus the huss-based vpr for each time period.

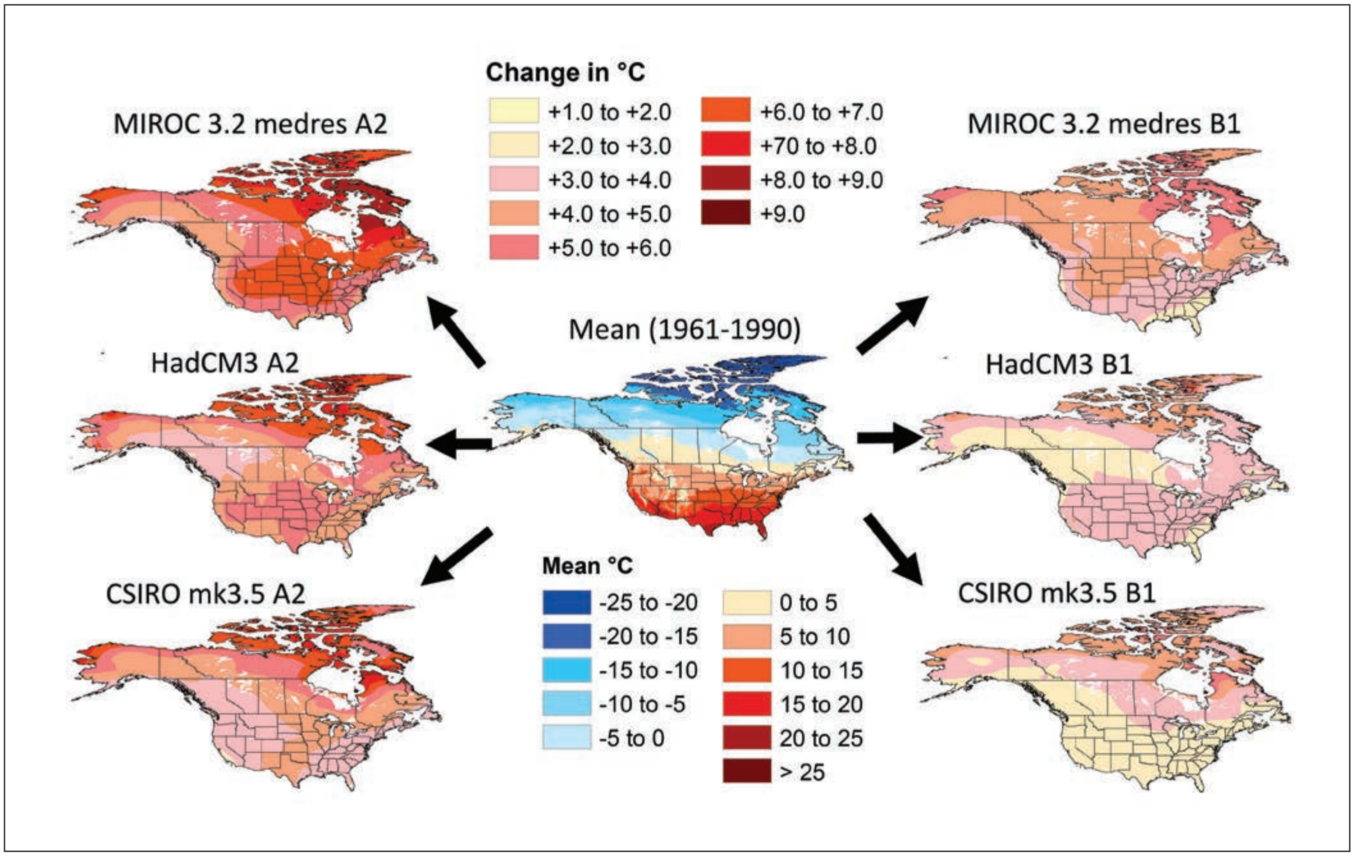

Figure 7—Mean monthly temperature levels for historical and six future scenarios. The map in the center is the average mean monthly temperature for the historical period (1961–1990). The maps along the sides show the mean temperature for the years 2070–2099 for the Special Report on Emissions Scenarios A2 and B1 emission scenarios for each climate model used in this study.

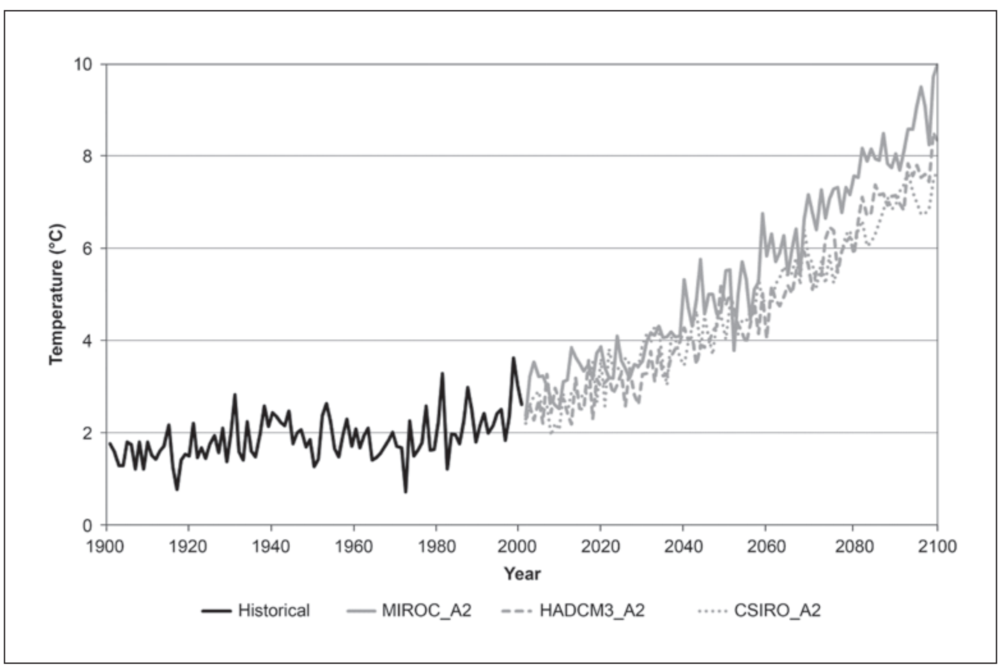

Figure 8—Area-weighted mean temperature across the United States and Canada by year in degrees Celsius for the three Special Report on Emissions Scenarios A2 future scenarios, with historical temperatures.

GCMs produce comparable levels of warming, with average temperature increases across the continent rising to close to 8 °C for the A2 emissions.

There is general agreement among all nine climate projections that precipitation increases in the 21st century in Alaska, most of Canada, the northern Rocky Mountains, and the northern Cascade Range (fig. 9). All nine climate projections show decreases in precipitation for most of Louisiana, the coastal plains of Texas, the south-central prairies of Kansas, and a patch of the western plains in Missouri. MIROC stands in contrast with the other GCMs in producing decreases in precipitation across most of the Eastern United States, south-central Canada, the western Great Plains, and the southern Great Basin. HadCM3 stands out from the

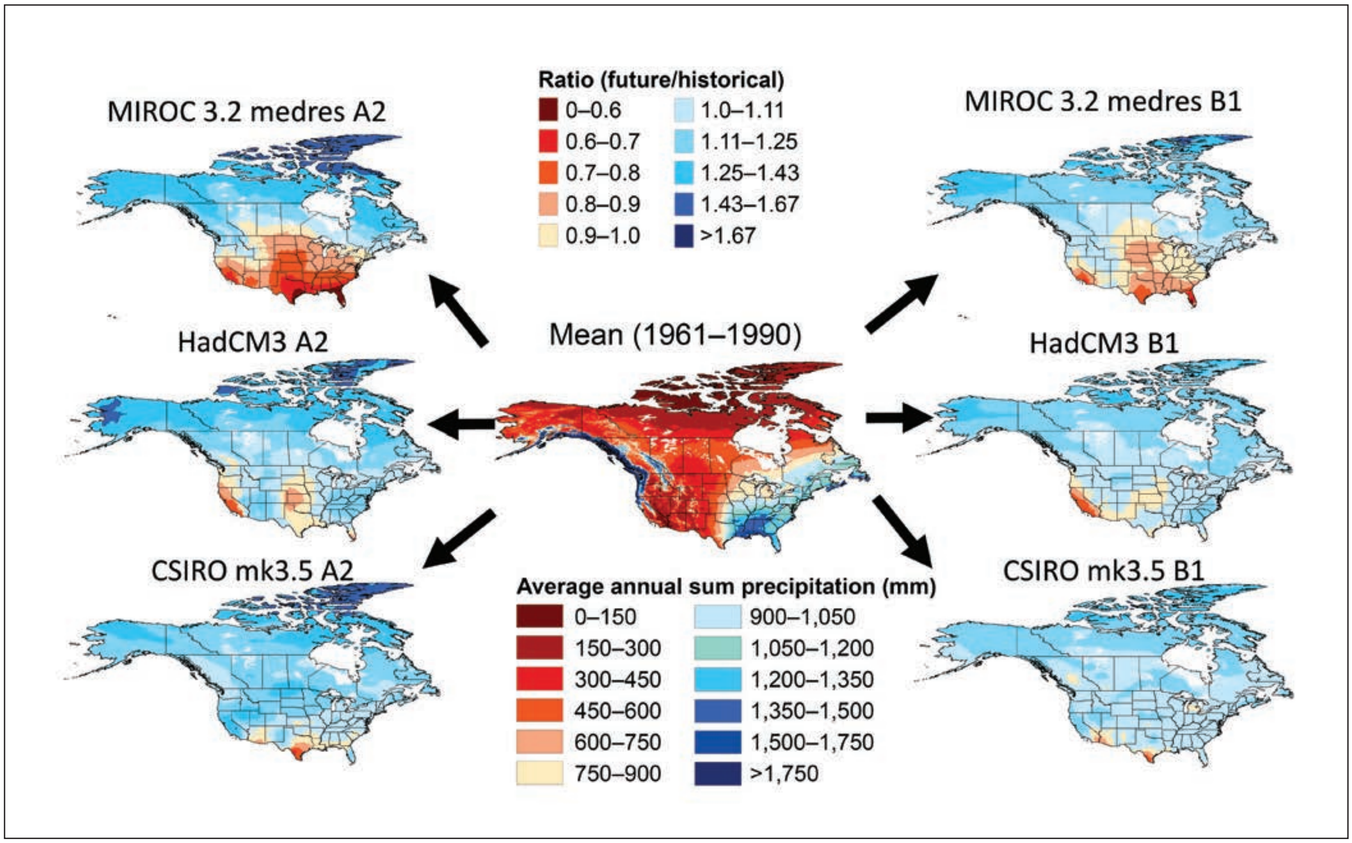

Figure 9—Mean monthly precipitation for historical and six future scenarios. The map in the center is the average annual sum precipitation for the years 1961–1990. The maps along the sides show the ratios of change in annual sum average precipitation for the years 2070–2099 versus 1961–1990 for the Special Report on Emissions Scenarios A2 and B1 emission scenarios.

other GCMs in projecting increases in precipitation in the Southwest and along the Gulf Coast. HadCM3 projects decreases in precipitation in western Oregon and Washington and in southern British Columbia. CSIRO differs from the other GCMs in projecting increases in precipitation in most of California, south-central Oregon, and across much of the Plains.

Temporal trends at the continental scale are somewhat divergent among the nine climate projections. HadCM3 and CSIRO A2 scenarios show a general trend of increasing precipitation throughout this century, with CSIRO producing much wider variation such that it includes both the highest and lowest precipitation levels of the 21st century (fig. 10). Though maps of MIROC precipitation show regions with dramatic decreases in precipitation, MIROC's precipitation average for the continent remains relatively flat through the 21st century for the A2 scenario.

MC1 Historical Outputs

To compare the Küchler (1964) potential vegetation map with MC1 simulated vegetation type distributions for the historical period (1961–1990), we created a crosswalk table associating Küchler and MC1 vegetation types (table 4). Vegetation types are determined annually in the MC1 model and can change from year to year. For spatial comparisons of MC1 versus Küchler, we used the mode vegetation map

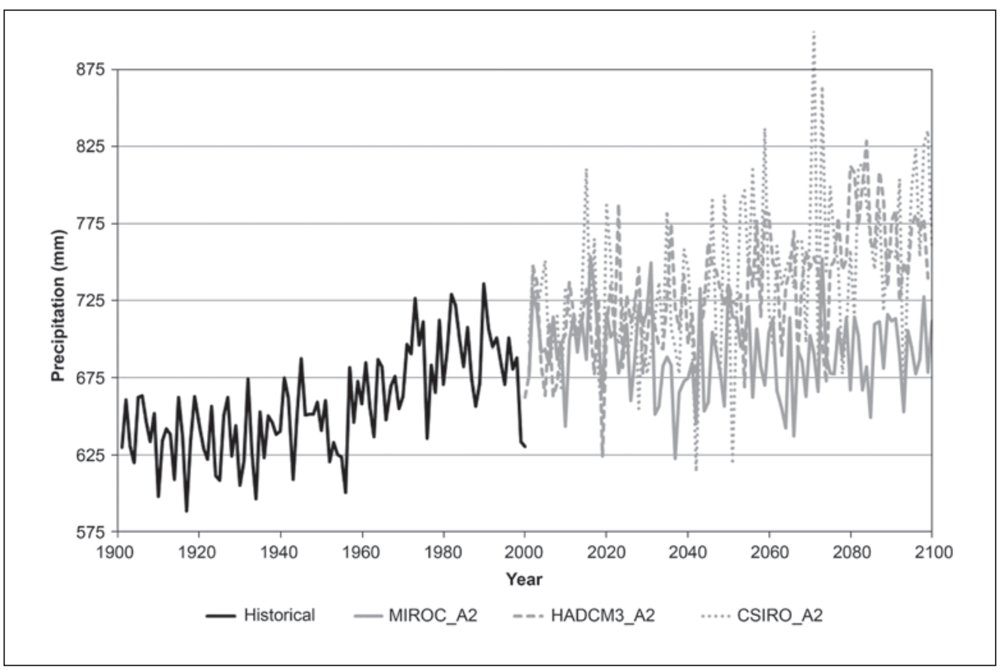

Figure 10—Area weighted mean annual sum precipitation averaged across the United States and Canada by year in millimeters for the three Special Report on Emissions Scenarios A2 future scenarios and for historical values.

Table 4—Crosswalk between Küchler, MC1, and an aggregated vegetation class

Küchler	MC1	Aggregated
	1 Ice/Barren	1 Ice/Barren
52 Alpine meadows and barren	2 Tundra	2 Tundra
93 Great lakes spruce/fir	4 Boreal Evergreen Needleleaf Forest	3 Forest
95 Great Lakes pine forest		
94 Conifer bog	5 Boreal Mixed Woodland	
4 Fir/hemlock	6 Subalpine	
7 Red fir forest		
8 Lodgepole pine/subalpine		
15 Western spruce/fir		
20 Spruce/fir/Douglas-fir		
21 Southwest spruce/fir		
22 Great Basin pine forest		
1 Spruce/cedar/hemlock	7 Maritime Evergreen Needleleaf Forest	
2 Cedar/hemlock/Douglas-fir		
3 Silver fir/Douglas-fir		
5 Mixed conifer		
6 Redwood		
9 Pine-cypress forest		
10 Ponderosa shrub	8 Temperate Evergreen Needleleaf Forest	
11 Western ponderosa		
12 Douglas-fir		
13 Cedar/hemlock/pine		
14 Grand fir/Douglas-fir		
16 Eastern ponderosa		
17 Black Hills pine		
18 Pine/Douglas-fir		
19 Arizona pine		
96 Northeastern spruce-fir forest		
97 Southeastern spruce-fir forest		

Table 4—Crosswalk between Küchler, MC1, and an aggregated vegetation class (continued)

Küchler	**MC1**	**Aggregated**
25 Alder-ash forest	9 Temperate Deciduous Broadleaf Forest	3 Forest
98 Northern floodplain		
99 Maple/basswood		
100 Oak-hickory forest		
101 Elm/ash		
102 Beech/maple		
103 Mixed mesophytic		
104 Appalachian oak		
106 Northern hardwoods	10 Temperate Cool Mixed Forest	
107 Northern hardwoods/fir		
Northern hardwoods/spruce		
109 Transition between #104 and #106		
110 Northeastern oak/pine		
26 Oregon oak woods	11 Temperate Warm Mixed Forest	
28 Mosaic of #2 and #26		
111 Oak/hickory/pine		
113 Southern floodplain forest		
105 Mangrove	21 Subtropical Evergreen Broadleaf Forest	
27 Mesquite bosques	22 Subtropical Mixed Forest	
29 California mixed evergreen forest		
112 Southern mixed forest		
2114 Pocosin		
115 Sand pine scrub		
116 Subtropical pine forest		
24 Juniper steppe woodland	12 Temperate Evergreen Needleleaf Woodland	4 Woodland
83 Cedar glades		
71 Shinnery	13 Temperate Deciduous Broadleaf Woodland	
81 Oak savanna		
82 Mosaic of #74 and #100		
84 Cross timbers		

Table 4—Crosswalk between Küchler, MC1, and an aggregated vegetation class (continued)

Küchler	MC1	Aggregated
89 Blackbelt	13 Temperate Deciduous Broadleaf Woodland	4 Woodland
30 California oakwoods	26 Subtropical Mixed Woodland	
31 Oak/juniper woodland		
32 Transition between #31 and #37		
85 Mesquite/buffalo grass		
86 Juniper/poak savanna		
87 Mesquite/oak savanna		
90 Live oak/sea oats		
91 Cypress savanna		
36 Mosaic of #30 and #35		
23 Juniper/pinyon woodland	37 Coniferous xeromorphic woodland	
37 Mountain mahogany/oak scrub	16 Temperate Shrubland	5 Shrubland
38 Great Basin sagebrush		
39 Blackbrush		
40 Saltbrush/greasewood		
55 Sagebrush steppe		
33 Chaparral	27 Subtropical Shrubland	
34 Montane chaparral		
35 Coastal sagebrush		
41 Creosote bush		
42 Creosote bush/bursage		
44 Creosote bush/tarbush		
45 Ceniza shrub		
62 Mesquite/live oak savanna		
49 Tule marshes	17 Temperate Grassland	6 Grassland
50 Fescue/wheatgrass		
51 Wheatgrass/bluegrass		
56 Wheatgrass/needlegrass shrubsteppe		
63 Foothills prairie		
64 Grama/needlegrass/wheatgrass		

Table 4—Crosswalk between Küchler, MC1, and an aggregated vegetation class (continued)

Küchler	MC1	Aggregated
66 Wheatgrass/needlegrass	17 Temperate Grassland	6 Grassland
67 Wheatgrass/bluestem/needlegrass		
68 Wheatgrass/grama/buffalo grass		
73 Northern cordgrass prairie		
74 Bluestem		
75 Nebraska sandhills prairie		
47 Fescue/oatgrass	28 Subtropical Grassland	
48 California steppe		
53 Grama/galleta steppe		
54 Grama/tobosa prairie		
57 Galleta/three awn shrubsteppe		
58 Grama/tobosa steppe		
59 Trans-pecos shrub savanna		
60 Mesquite savanna		
61 Mesquite/acacia savanna		
65 Grama/buffalo grass		
69 Bluestem/grama		
70 Sandsage/bluestem		
72 Sea oats prairie		
76 Blackland		
77 Bluestem/sacahuista		
78 Southern cordgrass prairie		
79 Palmetto prairie		
80 Marl-Everglades		
88 Fayette prairie		
92 Everglades		
46 Desert (vegetation absent)	18 Temperate Desert	7 Desert
43 Paleoverde/cactus	29 Subtropical Desert	

for the years 1961–1990 for a run of the MC1 model without fire suppression. The proportion of agreement between MC1 and Küchler was 0.61 for the aggregated vegetation classes and the Kappa coefficient was 0.51 (fig. 11). It is not possible to determine statistical significance to the Kappa coefficient, but Landis and Koch (1977) in a subjective determination called Kappas of 0.41 to 0.6 a "moderate" level of agreement. MC1 simulates forest and woodland vegetation types farther into the prairie region than Küchler. Much of the Southwestern United States is simulated to be grassland in MC1, but is shrubland in Küchler. Some of the eastern prairie is simulated as shrubland by MC1, but represented as grassland in Küchler.

The National Biomass and Carbon Dataset for the year 2000 (NBCD2000) of Kellindorfer et. al (2012) includes a map of aboveground live carbon mass. NBCD2000 data are based on an empirical modeling approach that combined

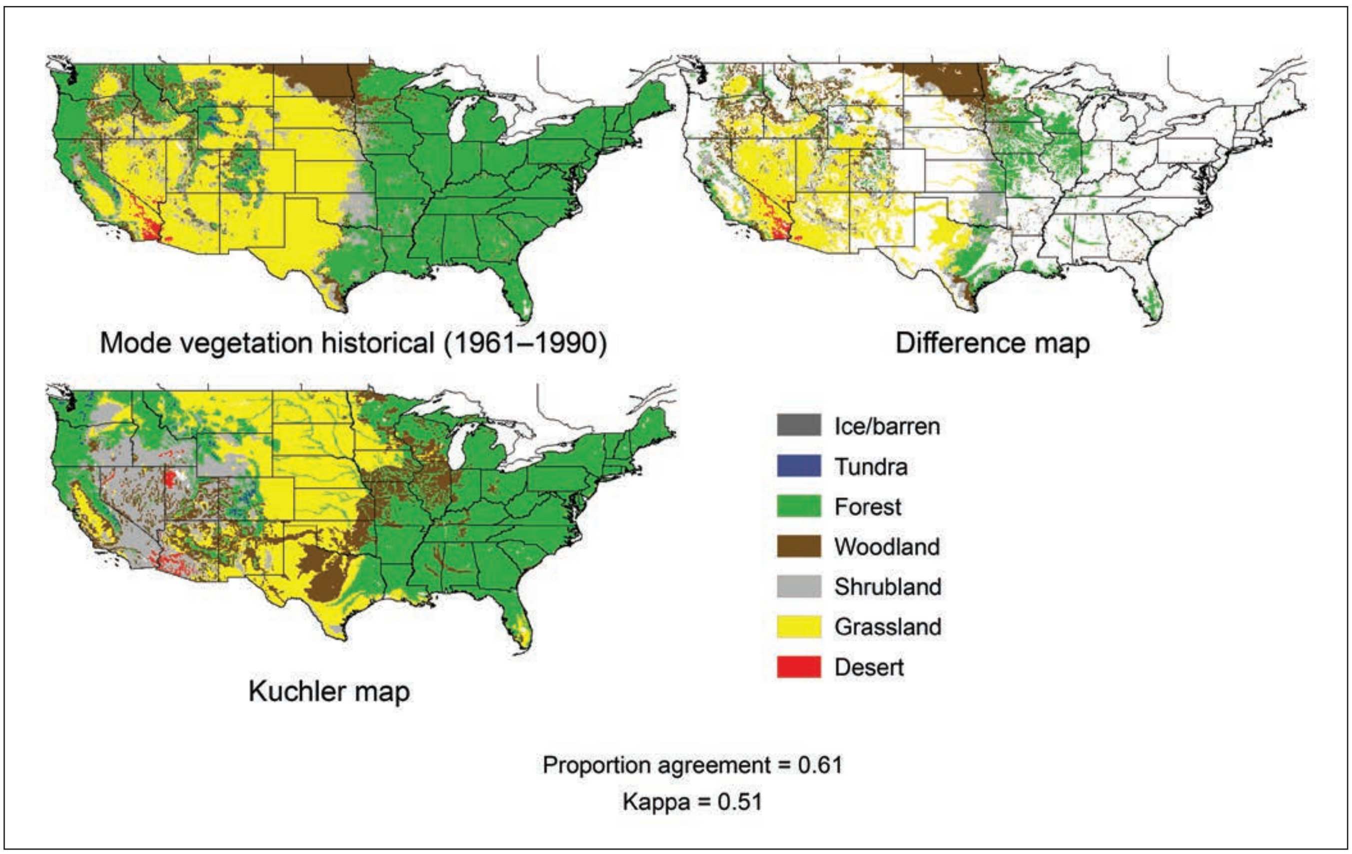

Figure 11—A comparison of the aggregated potential vegetation maps of MC1 and Küchler (1964). The MC1 map is the mode vegetation map for the years 1961–1990 for a run of the MC1 model without fire suppression. The difference map shows the MC1 aggregated vegetation classes where MC1 and Küchler differ.

USDA Forest Service Forest Inventory and Analysis (FIA) data with high-resolution InSAR remote sensing data acquired from the 2000 Shuttle Radar Topography Mission (SRTM) and remote sensing data acquired from the Landsat ETM+ sensor. We compared these NBCD2000 values against the results from MC1 for the sum of the variables aflivcx (maximum aboveground live tree carbon) and aglivcx (maximum aboveground live grass carbon).

The aboveground live carbon estimates from MC1 (aflivcx + aglivcx) are greater than NBCD2000 over 80 percent of the forested grid cells, with the greatest differences in the Coast Range of the Pacific Northwest, northern New England, and Florida (fig. 12). Locations where simulated vegetation carbon is relatively low are scattered across the map. There is a concentration near the Appalachian Mountains, along the Mogollon Rim in Arizona, along the Sierra Nevada in California, and up the Cascade Range in Oregon and Washington. But for most of the Rocky Mountains, MC1 live carbon is relatively high.

A significant potential cause for aboveground vegetation carbon differences is the fact that the NBCD2000 data are based on actual vegetation, whereas MC1 simulates potential vegetation. A scatterplot of MC1 versus NBCD2000 aboveground live carbon values within national parks provides more of an appropriate comparison (fig. 13). The best-fit line is parallel with the 1:1 line, and the slope is very close to 1.0. On average, MC1 produces values that are roughly 2,200 g m^{-2} higher than the NBCD values at all carbon levels.

We compared MC1's simulated fire return interval (FRI) with those estimated by Leenhouts (1998). Leenhouts estimated preindustrial and expected wildland fire activity by using national land classification data (Küchler 1964) and known ecological FRIs. Leenhouts provides a minimum and a maximum FRI for each of the Küchler vegetation classes. For MC1 we calculated the FRI as:

$$\mathrm{FRI} = \mathrm{N} / \sum_{\mathrm{year}=1}^{\mathrm{N}} \mathrm{part\_burn} \qquad (2)$$

where
FRI = fire return interval,
N = number of years examined (100 years, 1901–2000), and
part_burn = portion of the grid cell burned.

We compared simulated FRI to the maximum and minimum FRI estimated by Leenhouts (fig. 14). MC1 generally produces shorter FRIs in the Southwest and along the western boundary of the Great Plains, while producing longer FRIs in

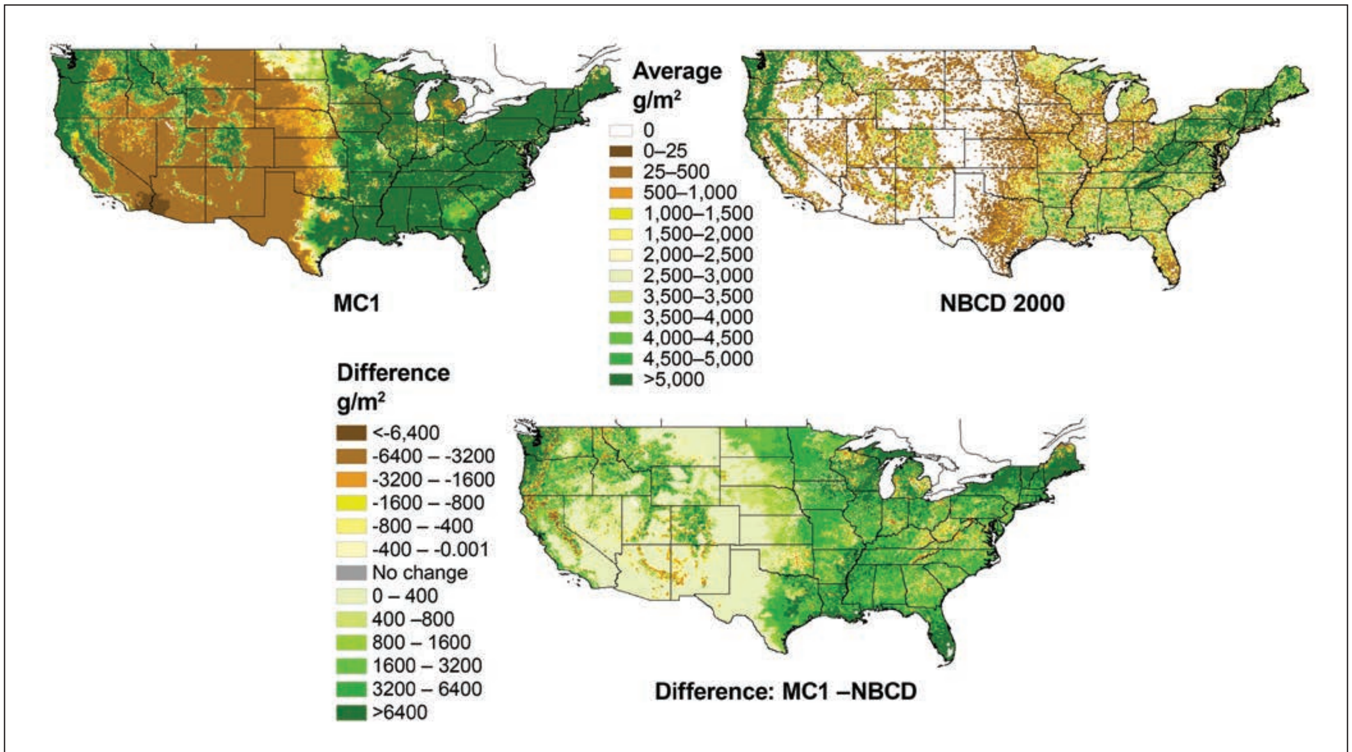

Figure 12—Maps of MC1 aboveground live carbon (grams per square meter) versus NBCD2000 (Kellindorfer et al. 2012) for the year 2000. To get aboveground live carbon, the MC1 variable aflivcx (maximum aboveground live tree carbon) was added to aglivcx (maximum aboveground live grass carbon). Also included is a difference map showing MC1 minus NBCD.

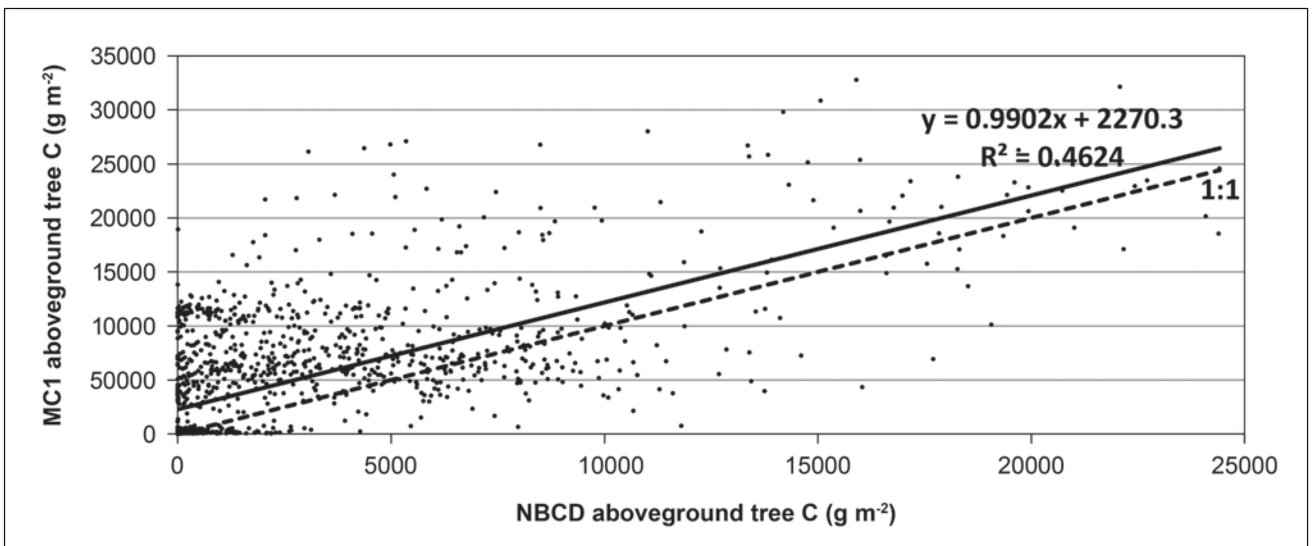

Figure 13—A scatterplot of MC1 aboveground live carbon versus NBCD2000 carbon (C) (Kellindorfer et al. 2012) on national park lands for the year 2000. To get the aboveground live carbon for MC1, the variable aflivcx (max aboveground live tree carbon) was added to aglivcx (maximum aboveground live grass carbon). The national parks map was obtained from the National Atlas of the United States and the U.S. Geological Survey. In this map, the polygons represent the federal- and Indian-owned lands of 640 ac or more in the United States. The solid line on the scatterplot is the least squares regression line, and the dashed line shows the 1:1 line where MC1 and NBCD carbon values are equal.

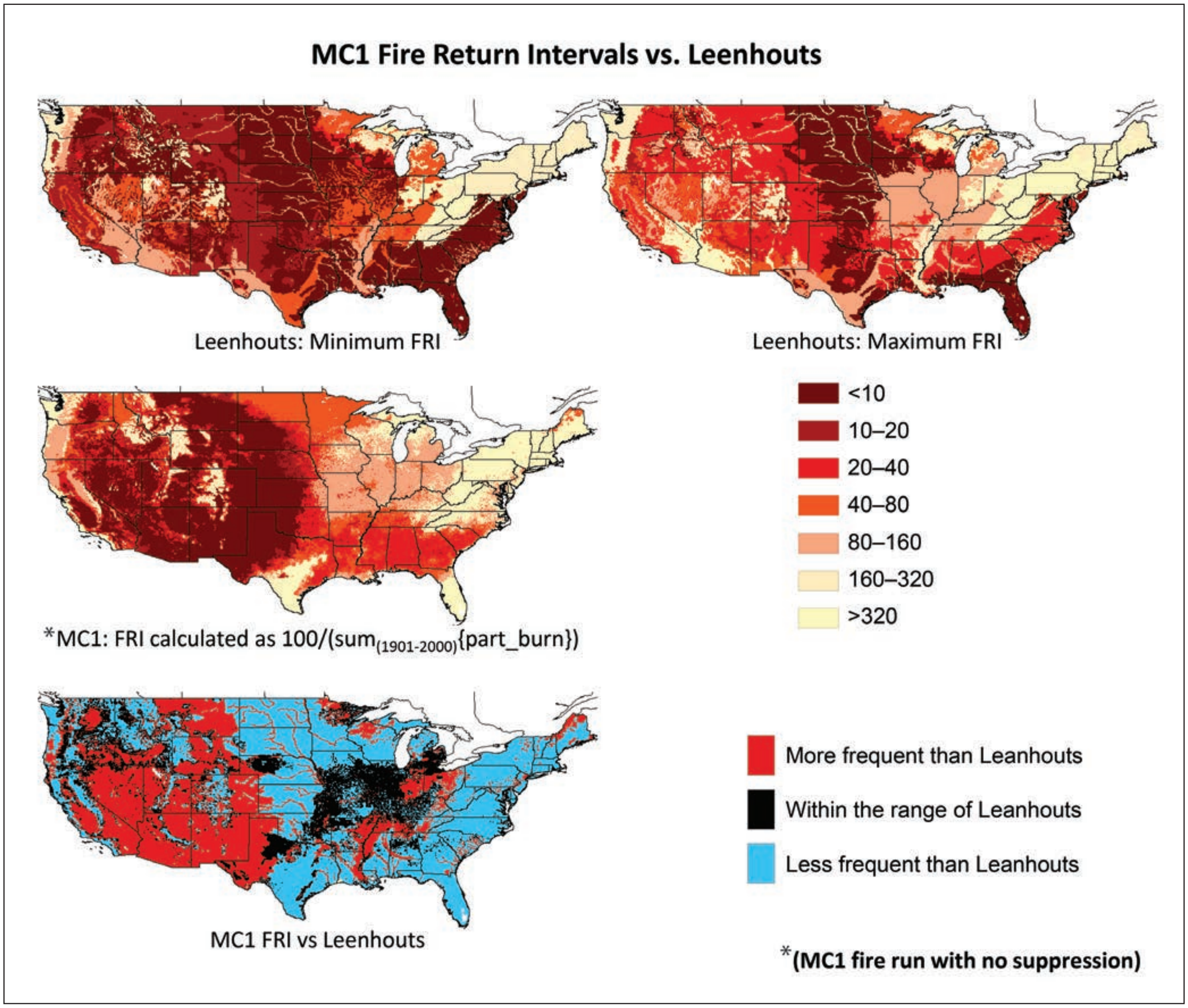

Figure 14—MC1 mean fire return intervals (FRI) versus minimum and maximum FRI published by Leenhouts (1998). Top maps are the Leenhouts minimum and maximum FRI. Center left map is the FRI from MC1 based on 50/(Σpart_burn)year = 1951,2000. Part_burn is the proportion of the grid cell burned. The bottom left map shows where the MC1 estimate falls within the Leenhouts range (black), where fires are more frequent with MC1 (red), and where they are less frequent (blue).

much of the Eastern United States and in the Northwest. In particular, MC1 simulates more frequent fires than Leenhouts across many of the relatively low-elevation areas in the West: the western prairies, southwest deserts, Great Basin, and Central Valley in California. MC1 also has higher frequency fires along the lower Mississippi River and in much of Ohio and Indiana. The area of the domain where the MC1 estimate of FRI falls within the range of Leenhouts is relatively small, comprising numerous patches in the Midwest, including the Prairie Peninsula, and smaller patches in the Northwest.

We compared MC1's simulated streamflow for the historical period against gage data for three basins in the United States: the Rogue River basin, Oregon; Salt River basin, Arizona; and Sinnamahoning Creek basin, Pennsylvania (table 5). The three basins were selected to ensure that at least several decades of streamflow gage data were available and to include one in the West with dry summers (Rogue River), one in the arid Southwest (Salt River Arizona), and one in the East (Sinnamahoning Creek). MC1's annual streamflow was calculated by summing annual streamflow for all grid cells within the basin boundaries. No routing or transport algorithms were applied. We compared streamflow for all the years for which gage data were available.

MC1 generally replicated streamflow with moderate skill. Of these three gages, the highest correlation between MC1 simulated flows and the gage was for the Salt River ($R^2 = 0.62$), but the model tended to overestimate streamflows (fig. 15). Average streamflow estimated by MC1 was closest to the gage average for the Rogue River, but the correlation was also the weakest ($R^2 = 0.33$). Correlation between simulated flows and the gage was intermediate ($R^2 = 0.49$) for Sinnamahoning Creek. MC1 appears to replicate the temporal variability of streamflow well, with some low and high biases at Sinnemahoning Creek and Salt River, respectively. For the Rogue River, MC1 tended to simulate flows that were too low during high-flow years and were too high during low-flow years. The low-bias at Sinnemahoning Creek is likely the result of MC1 overestimating the live vegetation in the basin, leading to greater interception evaporation and transpiration. Within the Sinnemahoning Creek basin, MC1 aboveground tree carbon values range from 106 to 226 percent of the NBCD2000 values. Another possible source of error is that the Sinnamahoning Creek drainage basin is small, having only nine grid cells

Table 5—Stream gages for which we compared streamflow

River	Rogue River	Salt River	Sinnamahoning Creek
Location	At Raygold near Central Point, Oregon	Near Roosevelt, Arizona	First Fork near Sinnamahoning, Pennsylvania
Gage number	14359000	09498500	01544000
Latitude	42°26'15"	33°37'10"	41°24'06"
Longitude	122°59'10"	110°55'15"	78°01'28"
Size of drainage basin (km^2)	5187	10 555	578
Average annual flow ($m^3 \times 10^8$)	26.9	8.1	3.6
Years covered	1906–1976	1913–2000	1956–2000

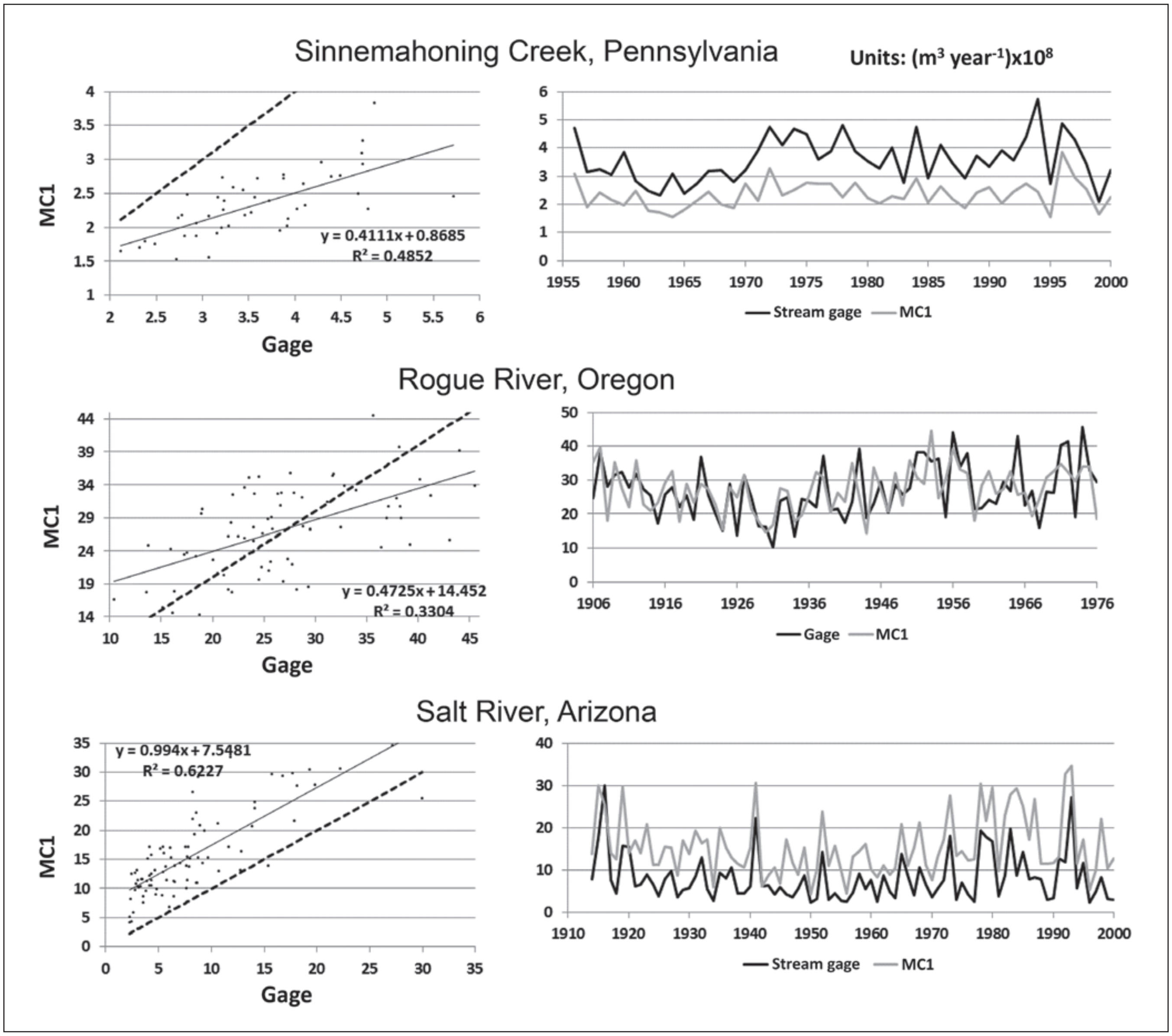

Figure 15—Measured streamflow versus that estimated by MC1 for three stream gages: the first fork of Sinnamahoning Creek near Sinnamahoning, Pennsylvania; the Rogue River at Raygold near Central Point, Oregon; and the Salt River near Roosevelt, Arizona. Plots on the left show MC1 estimates of annual streamflow (in m^3 $year^{-1}$ × 108) versus flow levels measured by the gage. Each point represents streamflow values for 1 year. The solid line shows the fitted least squares line through the points. The dashed line shows where the scatter would lie if the MC1 estimate and the measured streamflow were the same. Plots on the right show the annual sum flow rates over time with the black line being flows measured by the gage and the gray lines being estimates of flow from MC1 outputs.

fall within it. Delineating a drainage basin with grid cells will involve some error because some boundary grid cells will extend outside the drainage basin, and some areas along the edge of the drainage basin will not be included. For a small drainage basin such as Sinnamahoning Creek, the area where there are errors of omission and commission will be high relative to the area of the drainage basin.

MC1 Future Outputs

Changes projected by MC1 were more pronounced across GCMs than across the SRES emission scenarios (figs. 16 and 17). For each GCM, spatial patterns were relatively similar across all three emission scenarios, i.e., locations where model outputs increased and decreased relative to historical values were similar across the three emission scenarios. The A2 scenario produced the geographic pattern most strongly, the B1 scenario produced the pattern most weakly, and the A1B scenario was always intermediate. For example, of the three GCMs examined in this report, CSIRO is the only one to produce increases in streamflow in southern California (fig. 17), and those increases are most pronounced for the A2 emission scenario. In this report, emission scenario comparisons are primarily made between the B1 and the A2 scenario, and generally the CSIRO-B1 and the MIROC-A2 scenarios are used to represent the extremes of possible results.

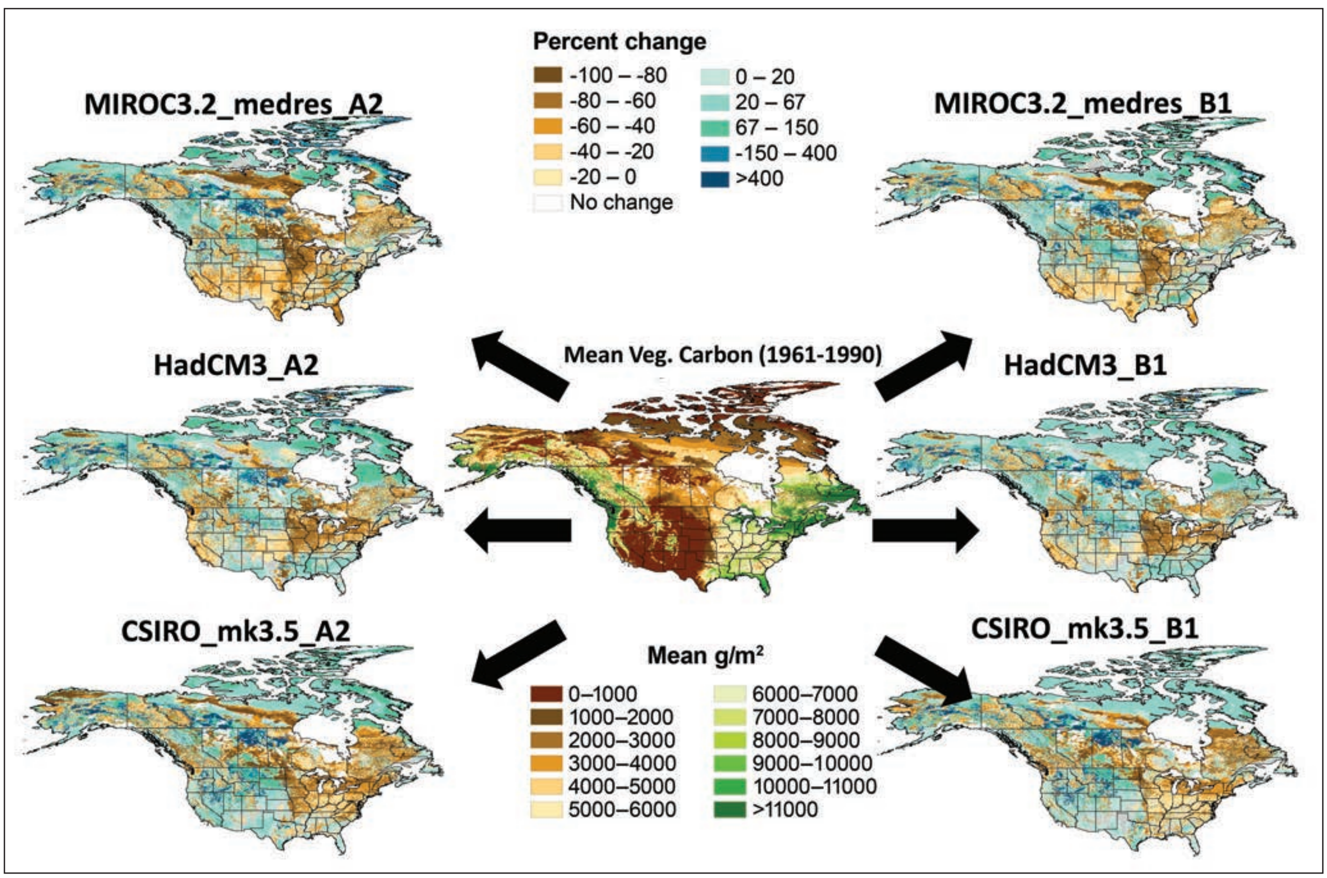

Figure 16—Change in vegetation carbon. The map in the center is the mean vegetation carbon for the years 1961–1990. The maps along the sides show the percentage change for the Special Report of Emissions Scenarios A2 and B1 emission scenarios where the percentage change is calculated as {((future – historical) × 100)/historical}. Future values were averages for the years 2070–2099.

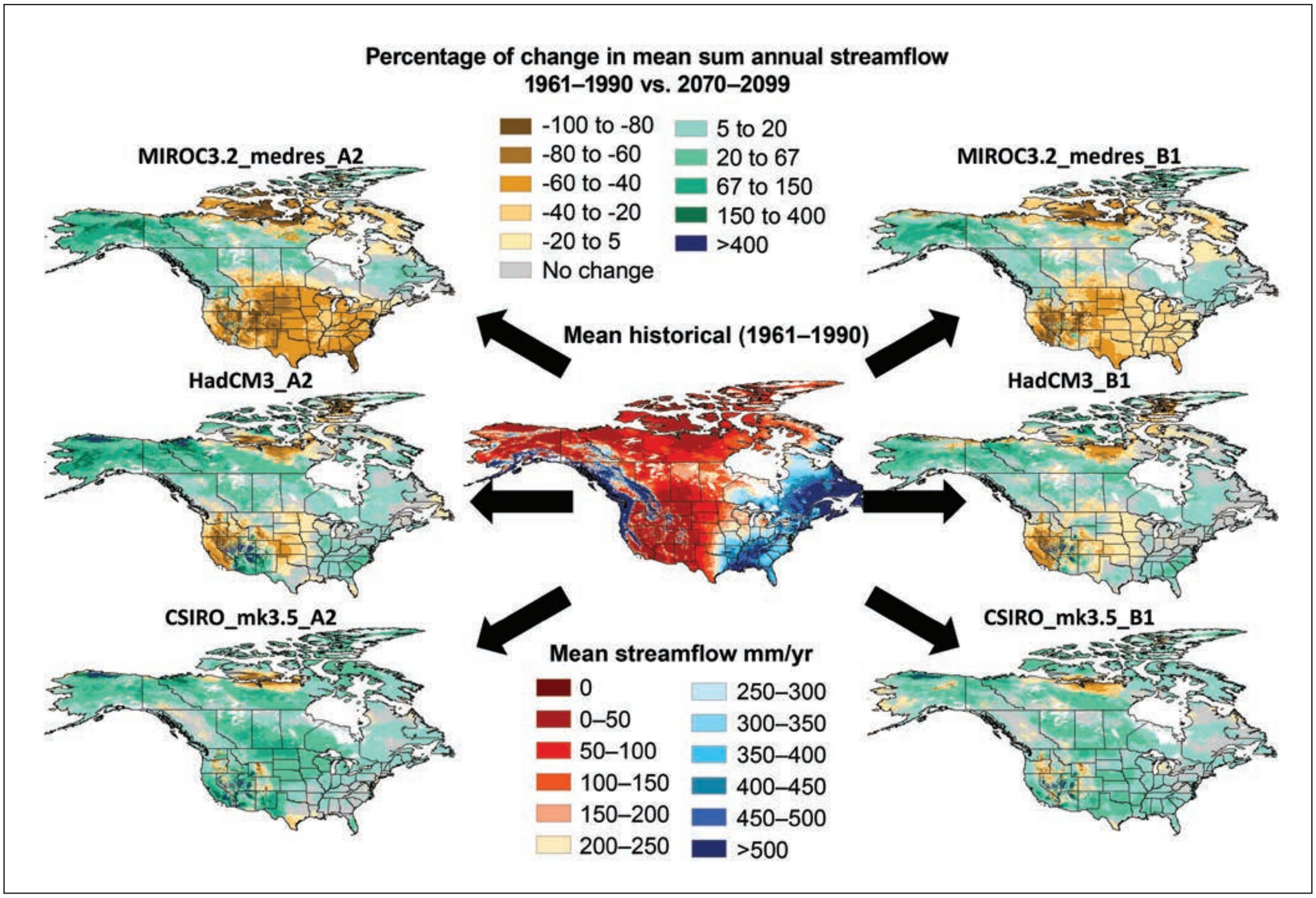

Figure 17—Mean annual streamflow derived from MC1 for the historical period, and the percentage change in streamflow for six future scenarios. The map in the center is the mean streamflow for the years 1961–1990. The maps along the sides show the percentage change maps for the Special Report on Emissions Scenarios A2 and B1 emission scenarios where percentage change is calculated as [((future – historical) × 100)/historical]. Future values were average for the years 2070–2099.

MC1 projects significant changes in the aggregated vegetation class by the end of the 21st century, with changes ranging from 37 percent of the total land area under CSIRO-B1 to 45 percent under MIROC-A2 (fig. 18). The most apparent shifts are from woody encroachment in the far northern regions (table 6). Of the area that starts as barren, 82 percent shifts to tundra for MIROC-A2, and 72 percent shifts for CSIRO-B1. Under MIROC-A2, 56 percent of the tundra is converted to forest or woodlands and 34 percent makes that conversion for CSIRO-B1. Under MIROC-A2, 57 percent of the woodlands converts to forests and 58 percent makes that conversion in CSIRO-B1. Most of these woodlands that shift are in the far north ("taiga-tundra" for the unaggregated vegetation class).

Looking at the vegetation classes of lower latitudes, 28 percent of the forests convert to less woody classes under MIROC-A2, and 22 percent of the forests make that conversion for CSIRO-B1. Most of the forest conversions happen in the

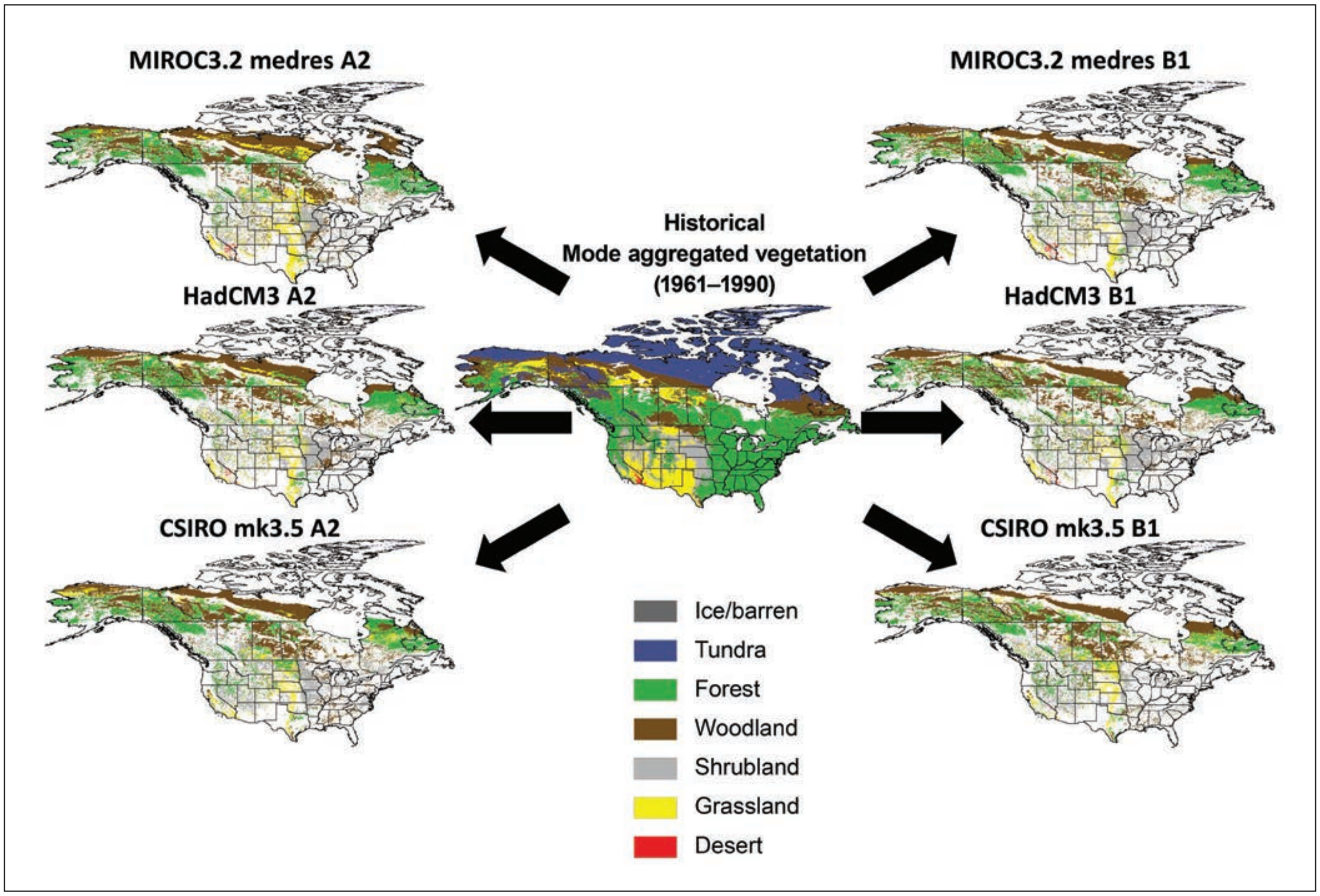

Figure 18—Change in vegetation class for an aggregated vegetation class. Center map shows the mode vegetation map for the years 1961–1990 (historical period). The maps along the sides show change maps for the Special Report on Emissions Scenarios A2 and B1 emission scenarios. The change maps show white where the historical and future maps are the same and show the future vegetation classes for locations where there are differences.

Table 6—Proportions of areas changing from one aggregated vegetation class to another for the two most extreme scenarios

MIROC A2 AREAS

		Barren	Tundra	Forest	Woodland	Shrubland	Grassland	Desert
Historical	Barren	0.18	0.82	0	0	0	0	0
	Tundra	0	0.36	0.20	0.36	0	0.07	0
	Forest	0	0	0.72	0.10	0.12	0.06	0
	Woodland	0	0	0.57	0.31	0.05	0.07	0
	Shrubland	0	0	0.10	0.06	0.44	0.40	0
	Grassland	0	0	0.03	0.24	0.17	0.55	0.01
	Desert	0.14	0	0.02	0	0	0.04	0.81

CSIRO B1 Areas

		Barren	Tundra	Forest	Woodland	Shrubland	Grassland	Desert
Historical	Barren	0.30	0.70	0	0	0	0	0
	Tundra	0	0.66	0.06	0.28	0	0.01	0
	Forest	0	0	078	0.11	0.09	0.02	0
	Woodland	0	0	0.58	0.23	0.04	0.14	0
	Shrubland	0	0	0.20	0.08	0.50	0.22	0
	Grassland	0	0	0.05	0.19	0.20	0.55	0
	Desert	0	0	0	0	0.05	0.23	0.72

Note: Values show changes from the historical period (1961–1990) to the future period (2070–2099). Each cell is the proportion of the area starting as the vegetation class indicated along the left of the table and switching to the vegetation class indicated along the top of the table. Each row should sum up to 1.0.

provinces of southern Canada, with most of the forests of the Eastern United States remaining as forests, although when unaggregated vegetation classes are examined, conversions to different forest types do occur. At mid-latitudes (southern Canada and northern United States), most woodland areas that change convert to grasslands, with 14 percent of the original area converting to grasslands for CSIRO-B1. Areas that start as shrubland and switch to another vegetation class go both in the direction of more wood and of less wood. For MIROC-A2, most shrubland areas that switch convert to grasslands (40 percent), whereas only 16 percent convert to forests or woodlands. For CSIRO-B1, 22 percent of the area that changes converts to grasslands and 28 percent converts to forests or woodlands. For MIROC-A2, 44 percent of the area starting as grasslands converts to more woody vegetation classes, and 45 percent makes that shift for CSIRO-B1. Of the areas that start as desert, 14 percent converts to a more arid category (barren) for MIROC-A2, and 23 percent converts to a less-arid category (grassland) for CSIRO-B1. There are two types of barren land that get lumped in MC1: cold barren (ice fields) and hot barren (desert areas so extreme as to be almost completely lacking in vegetation). Most of the conversions from barren in table 6 are for cold barren areas converting to tundra, and most of the conversions to barren are from desert to hot barren.

Gonzalez et al. (2010) used shifts in MC1 vegetation type output as one indicator of ecosystem vulnerability. He created a map showing the number of scenarios where the vegetation type shifts for every grid cell. The assumption is that, for each grid cell, the higher the number of scenarios that lead to type shifts, the more "vulnerable" is its ecosystem. We created the same type of map (fig. 19) by using our MC1 results for the nine scenarios. According to our map, the most "vulnerable" ecosystems were located in the northern part of the continent along ecotones, especially along the forest-tundra ecotone and along the forest-grassland ecotone. Most of Southeastern United States is projected to remain forested, but changes from one forest type to another are projected to occur. Most of the desert regions of the Southwest were projected to remain unchanged, as were the forests of western

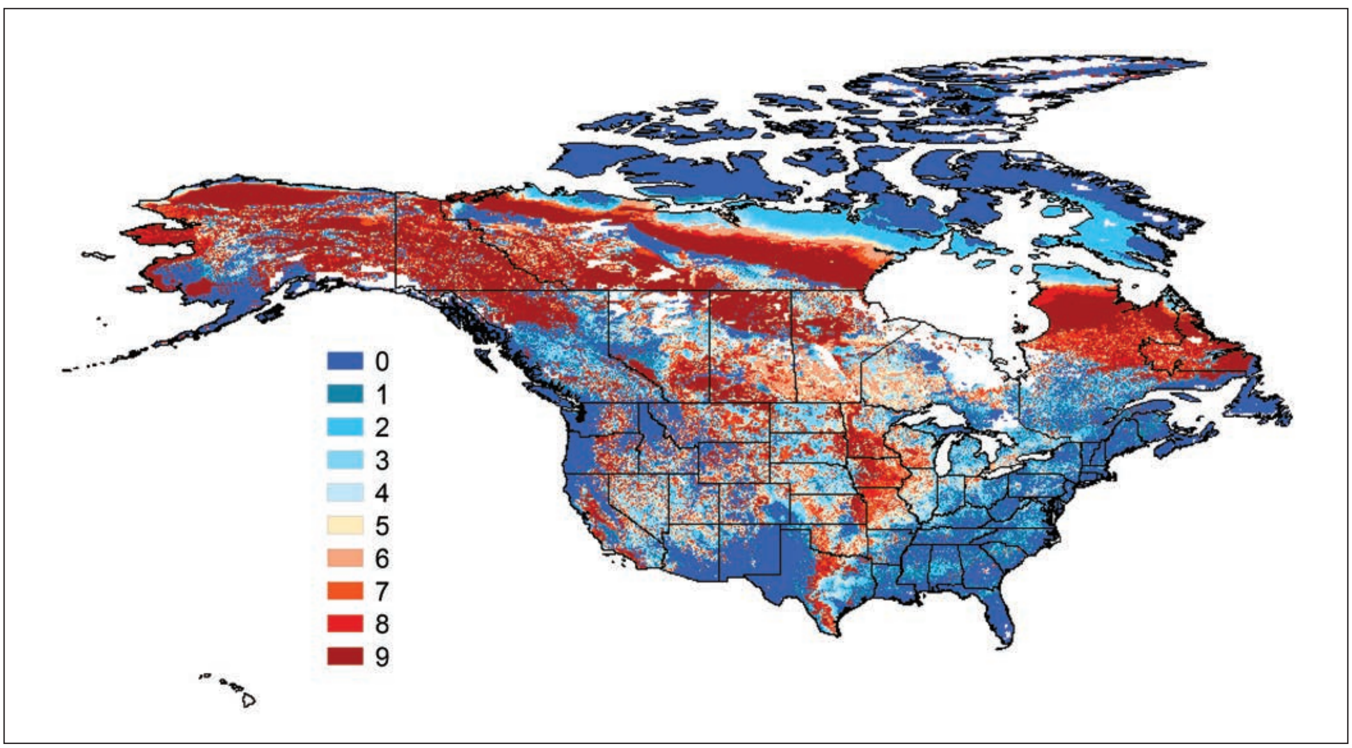

Figure 19—The number of future scenarios (out of nine) where the aggregated vegetation class changes. The aggregated vegetation class consists of six basic classes: cold, forest, woodland, savanna, grassland, and shrubland.

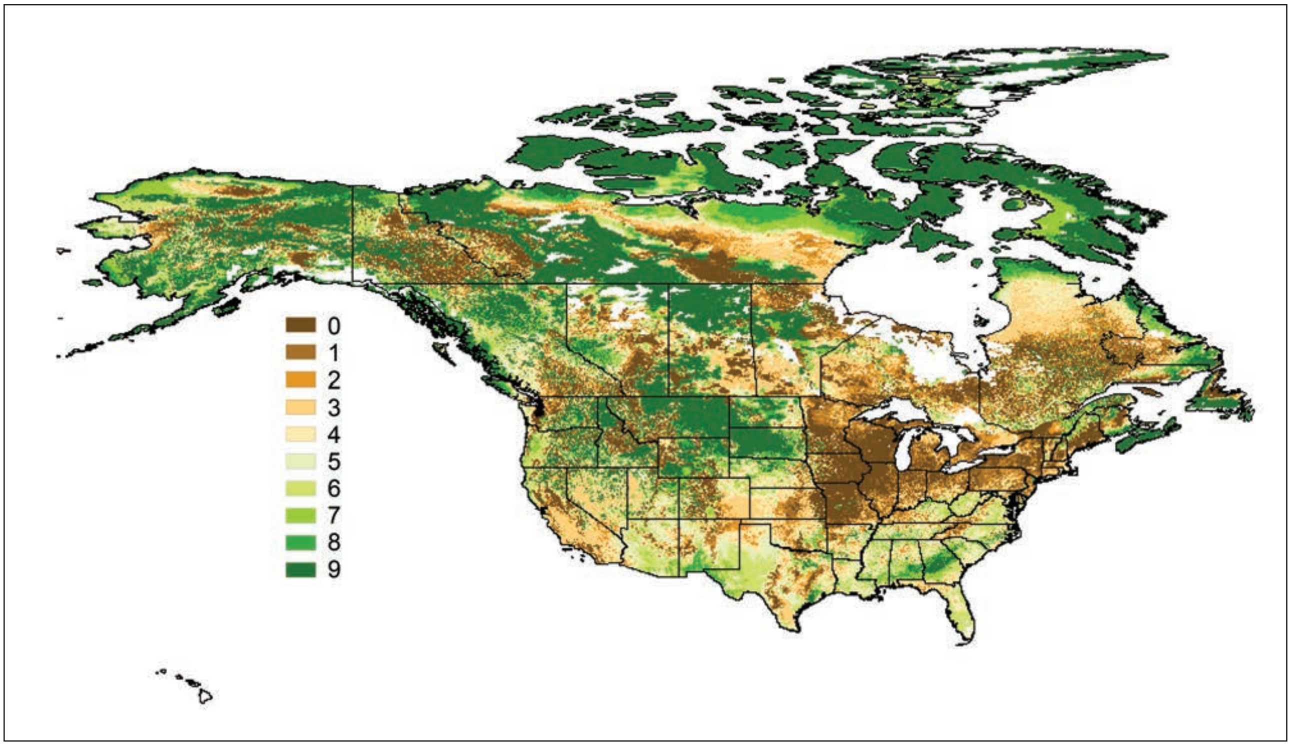

Figure 20—The number of future scenarios (out of nine) in which the average vegetation carbon increases relative to the historical period. Average historical vegetation carbon is calculated for the years 1961–1990, and average future vegetation carbon values are calculated for the years 2070–2099.

Oregon and Washington. This map is not intended to suggest that those areas have no vulnerabilities under climate change scenarios. For example, even within MC1 results, some of those areas experience large increases in fires under some scenarios.

For vegetation carbon, there is broad agreement of geographic patterns among all simulation results. Far northern regions of Canada generally increase in vegetation carbon (fig. 20). These regions correspond to locations where forests encroach on tundra. Vegetation carbon in the northern Plains states generally increases as well, and this corresponds to shrub encroachment on grasslands. All simulation results produce decreases in vegetation carbon from the Midwestern United States through Michigan and northern Ohio to the Northeastern United States. Decrease in vegetation carbon continues northward into much of southeastern Ontario and Quebec, though it is a bit more scattered in the Canadian provinces. Much of this decrease is due to conversions of forest to woodland or shrubland types. MIROC diverges from the other two GCMs in forecasting a greater decrease in vegetation carbon in the Southern United States (fig. 16). HadCM3 differs from the other GCMs in producing downward trends in vegetation carbon in western Oregon and

Washington, but HadCM3 shows more increases in the plains provinces of Canada and in the Southeastern United States than do the other two GCMs. CSIRO is unique in that it shows increases in vegetation carbon in California and Nevada, as well as in the plains states of Nebraska, Kansas, Oklahoma, and eastern Colorado. It is the one GCM to show decreases in the central Atlantic States.

All simulated scenarios forecast a decline in average vegetation carbon for the continent from the present to the end of the 21st century (fig. 21). Simulation results using HadCM3's climate projections forecast the most stable vegetation carbon, with results from the B1 scenario being the most stable after mid-century. Simulations using MIROC's climate projections cause steadier carbon losses than HadCM3. Simulations using CSIRO's climate projections cause a very rapid vegetation carbon decline in the first half of the 21st century, followed by a rise in the second half. Note that all scenarios end the 21st century with average vegetation carbon levels that exceed those of the start of the 20th century, but also note that the model does not include pests or pathogens.

The analysis of changes in the biomass consumed by fire projected by MC1 is complicated by the widely varying ranges simulated for historical values, from virtually no fire at all to over 400 g C^{-1} m^{-2} on average. For this reason, the percentage of change maps (fig. 22) need to be interpreted with some caution. Some large-percentage increases represent large increases in absolute terms, whereas for other grid cells with very little historical fire, a large-percentage increase corresponds

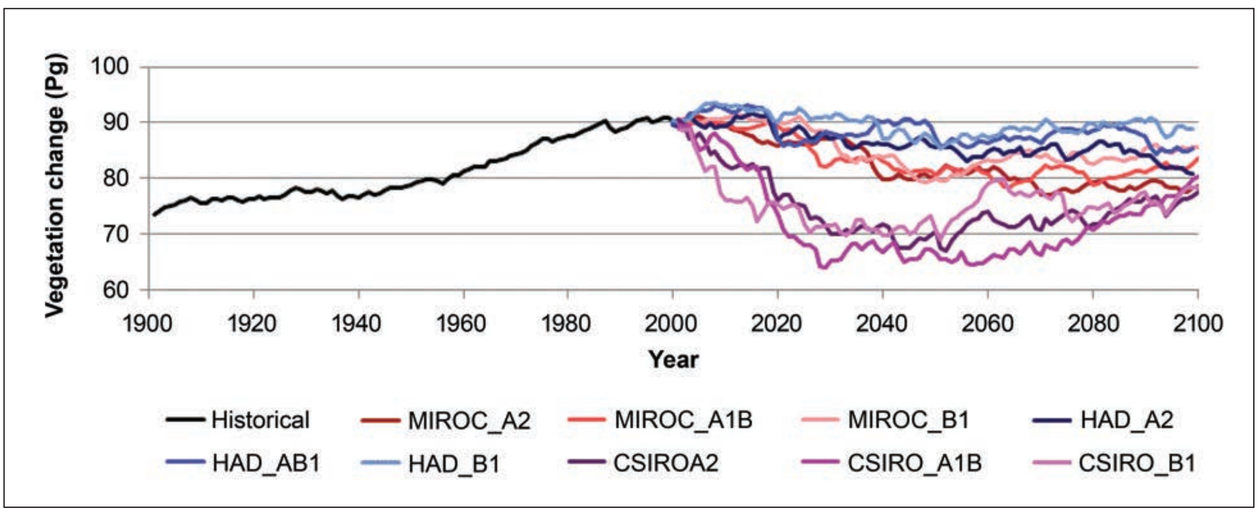

Figure 21—Total vegetation carbon across the United States and Canada by year in petagrams (Pg) for the nine future scenarios and for the historical period. MC1 vegetation carbon output is in grams of carbon per square meter. The area of each grid-cell, calculated in square meters, was multiplied by the vegetation carbon biomass consumed output value to produce the biomass consumed in grams and these values were summed across all grid cells.

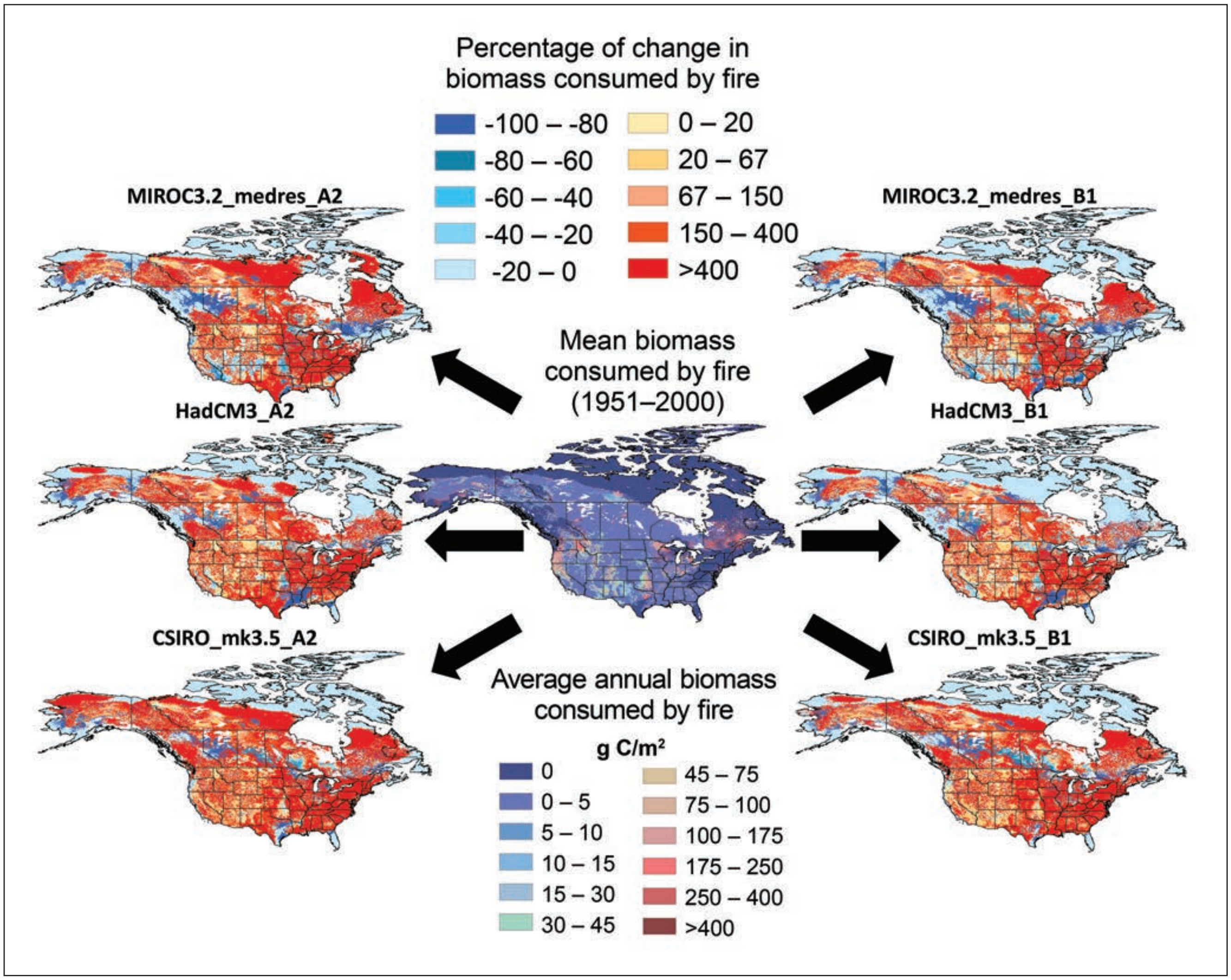

Figure 22—Average biomass consumed by fire coming from MC1 for the historical period and the percentage change in biomass consumed by fire for six future scenarios. The map in the center is the average biomass consumed by fire for the years 1951–2000. The maps along the sides show the percentage change maps for the Special Report on Emissions Scenarios A2 and B1 emission scenarios where percentage change is calculated as (future – historical) × 100)/historical. Future values were averages for the years 2050–2099.

to little change in absolute amounts (grams of carbon per square meter). Generally there is agreement among all scenarios that biomass consumed by fire will increase for most areas of the United States and Canada. Increases generally do not occur in Alaska and Canada, where virtually no fire is simulated for the historical period. Another region lacking consistent increases across all scenarios lies along the Gulf Coast. There are no locations across the entire study area where all scenarios project decreases in biomass consumed.

Time series of average biomass consumed averaged across the study area produce some startling results (fig. 23). All three GCMs produce frequent fire events in the 21st century that are bigger than anything simulated historically, but CSIRO

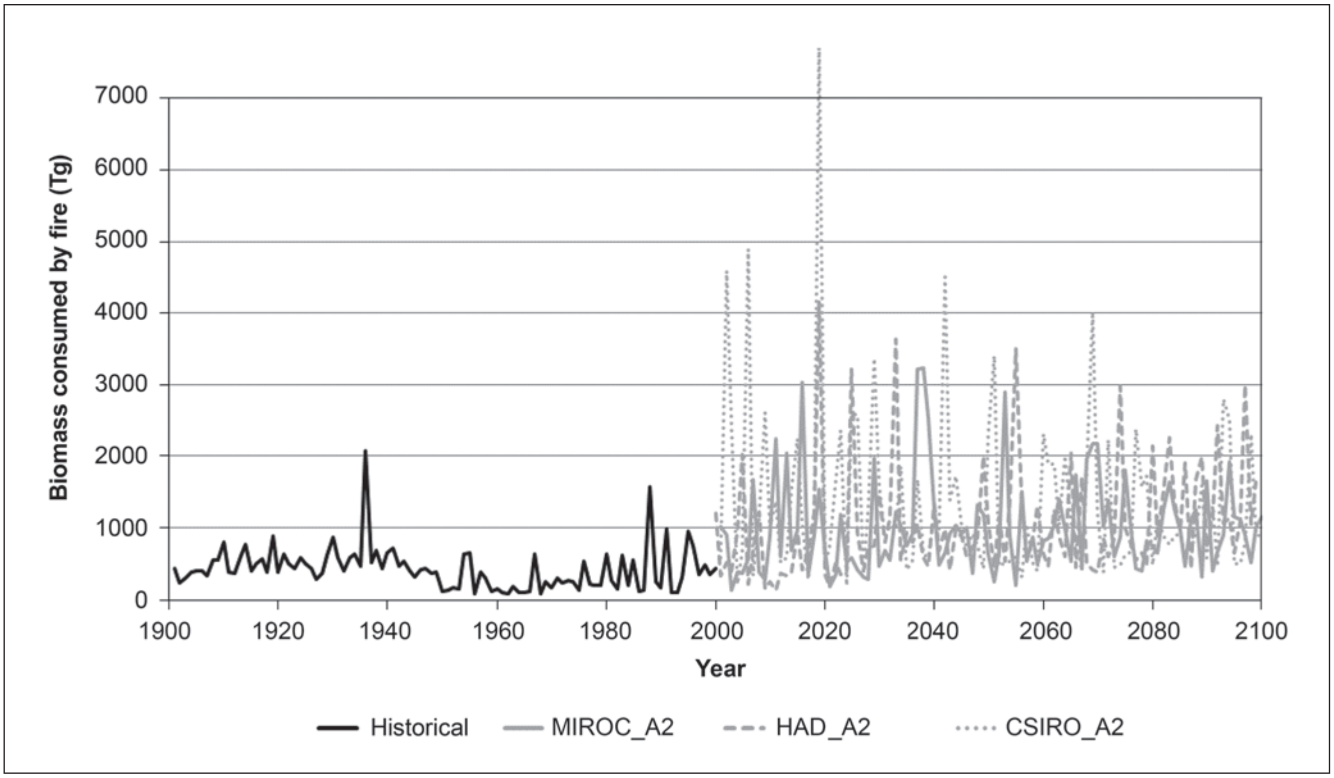

Figure 23—Total biomass consumed by fire across the United States and Canada by year in teragrams (Tg) for the nine future scenarios and for the historical period. Output of biomass consumed by fire for the MC1 model is in units of grams of carbon per square meter. The area of each grid cell, calculated in square meters, was multiplied by the biomass consumed output value to produce the biomass consumed in grams, and these values were summed across all grid cells.

produces some extraordinarily large fire events starting from the very first decade. For these datasets, historical data end with the year 2000, and from 2001 onward the model is run on downscaled GCM climate. This means that as of this writing, we are over a decade into the "future" scenarios. The large conflagrations predicted by using CSIRO climate projections have not yet been observed. It is difficult to say whether this results from an error in the climate projection or in the projection of fires coming out of MC1.

There is general agreement among the scenarios that streamflow increases in the 21st century in Alaska and in much of northern Canada (fig. 17). The scenarios all agree that much of eastern Oregon and Washington have decreases in streamflows as have much of central Wyoming and Colorado. MIROC produces the most pronounced decreases, and stands in contrast with the other two GCMs in producing decreases across most of the Eastern United States and in parts of southeastern Canada. It also is alone in producing decreases in Arizona and New Mexico as well as in much of Montana and southern Alberta and Saskatchewan. HadCM3 stands out from the other two GCMs in producing decreases in streamflow in northwestern Oregon, through much of Washington, and in southern British Columbia. CSIRO produces the most increases in streamflow and stands out from the other two scenarios in producing increases throughout the prairie states and in California and southwestern Oregon. These spatial patterns roughly correspond to those observed for changes in precipitation (fig. 9).

Though the MIROC scenarios produced pronounced decreases in streamflow regionally, average continental streamflow drops only slightly from the maximum level observed in the last quarter of the 20th century, and it never drops below levels observed in the 20th century (fig. 24). HadCM3 and CSIRO show moderate increases on average from late 20th-century levels, but with CSIRO displaying some occasional peaks that are much higher than ever observed in the 20th century. These temporal patterns roughly correspond to those observed for precipitation (fig. 10).

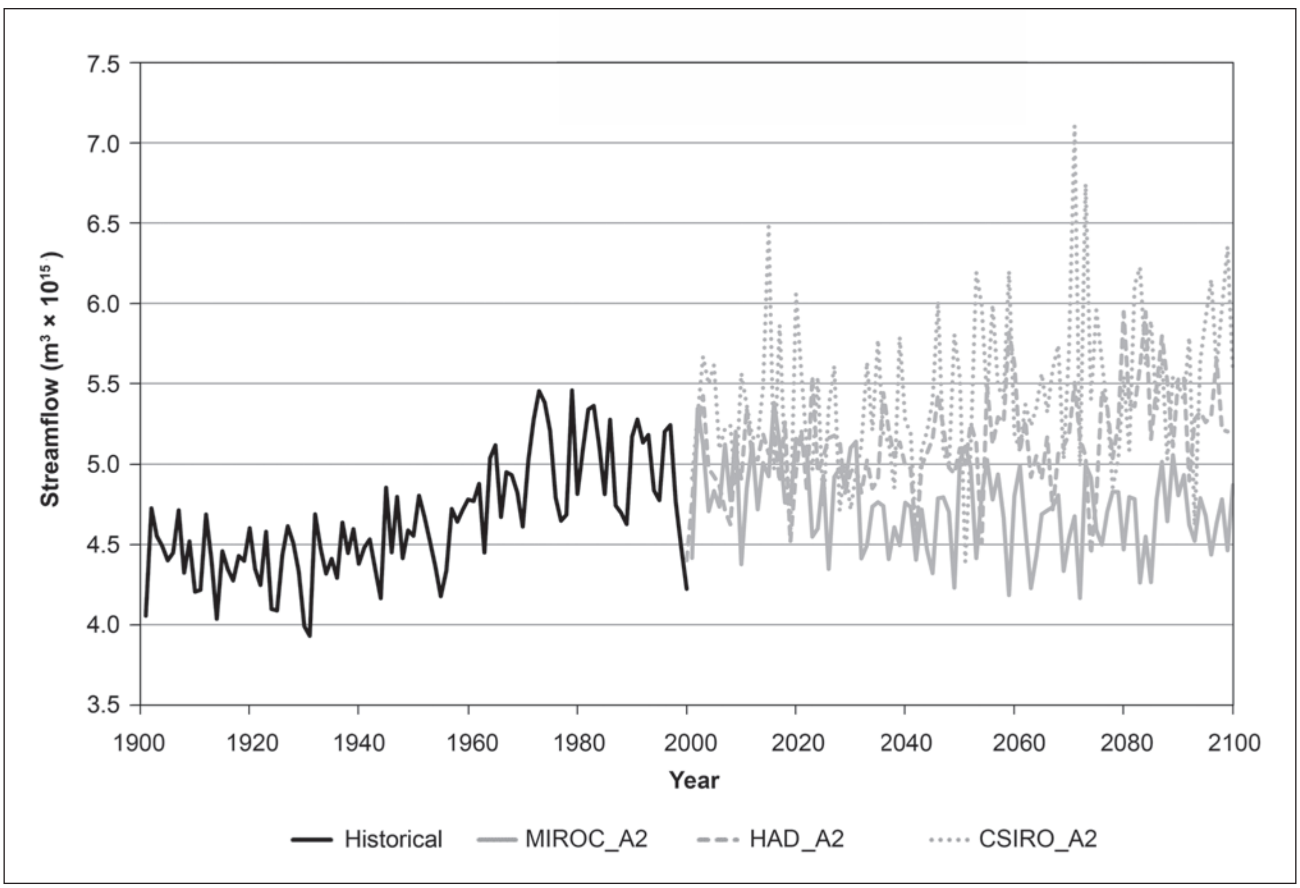

Figure 24—Total streamflow across the United States and Canada by year in $m^3 \times 1015$ for the nine future scenarios and for the historical period. The output of streamflow for the MC1 model is in units of millimeters per year. The area of each grid cell, calculated in square meters, was multiplied by the MC1 stream-flow to produce the streamflow in cubic meters per year, and these values were summed across all grid cells.

Discussion

Because vegetation biomass strongly influences both fire events and potential vegetation designations, it is important to model it skillfully. The NBCD2000 carbon data provide an important benchmark, but comparing MC1 aboveground vegetation carbon (AGVeg) with the NBCD2000 values raises an issue that is frequently encountered when comparing dynamic global vegetation models, such as MC1, against empirically measured benchmarks. MC1 simulates potential vegetation, whereas most benchmarks are modeled or measured from actual vegetation. With the NBCD2000 data, we were able to look at a comparison restricted to national parks, where the vegetation is more likely to represent potential natural vegetation (PNV) than elsewhere. The correlation between MC1 and NBCD2000 improves from an R^2 of 0.34 to 0.46 when we confine the comparison to just national parks. Although the national park mask we used for this comparison probably represents locations more like potential vegetation, many of those grid cells may have undergone some human disturbance.

Potential natural vegetation is defined as the last successional stage of native flora of an area under the current climate regime and lacking further human changes (Küchler 1964). This is a concept with several potential problems and subject to much discussion in the literature (Chiarucci et al. 2010, Somodi et al. 2012). It has been argued that the designations are subjective, scale dependent, and dependent on the timing of the observations used to make the designation. The PNV concept assumes that one final stage is reached in vegetation succession under stable conditions, but stable conditions are rarely reached in the real world. Because of these complexities, PNV types are difficult to simulate accurately for inherently dynamic ecosystems such as savannas and shrublands. Savannas consist of a mosaic in which clumps of woody plants are dispersed throughout a grassy matrix. Scholes and Archer (1997) noted:

> …all mixtures of mature trees and grass are unstable in savanna environments. In the absence of disturbances such as repeated fires, clearing by humans, or feeding by large herbivores, the tree cover increases at the expense of grass production until it is limited by tree-tree competition.

The maintenance of a savanna state is a dynamic process based on disturbance events that happen at scales smaller than the 5-arc-minute grid cell size used in this project. MC1 uses a modified version of the CENTURY Soil Organic Matter Model, which always runs in “savanna mode.” In “savanna mode,” the model always simulates both woody and grass biomass in every grid cell, with the woody biomass occasionally being decreased by fire events. MC1 does not model individual plants, and the PNV is determined annually. Therefore, the distinction among grasslands, shrublands, and savannas is determined solely by the amounts of woody and grass biomass in a given grid cell for a single year.

The dynamic balance that maintains savannas and the simplicity of MC1's algorithm for distinguishing savannas from other vegetation types help explain much of MC1's differences from benchmark data. For example, MC1 predicts more woody types in the eastern Great Plains and in the Prairie Peninsula, along with higher levels of simulated vegetation carbon. Anderson (1990) stated that "the prairie peninsula historically has fluctuated between a climate capable of supporting grassland and one supporting forest." Briggs et al. (2002) observed that "[the tallgrass prairie biome] occupies a tension zone between forest and grassland and historically this tension zone has been quite sensitive to shifts in climate, land management and fire regime." In recent years, the average climate has been capable of supporting forests (Anderson 1990), and because the PNV maps were published by Küchler (1964), there has been a considerable encroachment of woody vegetation in the areas of the tallgrass prairie (Lett and Knapp 2005).

Fire return intervals (FRI) for MC1 were calculated by summing the value for the part_burn variable, which represents the portion of the grid cell burned in a year (equation 2). This is consistent with the fact that most MC1 simulations heretofore were based on relatively large grid cell sizes of 0.5° latitude and longitude (Bachelet et al. 2001b, 2005), and such a large grid cell should not burn completely when a fire event is simulated. An alternative way of interpreting the part_burn variable is possible. Some recent projects have used relatively fine spatial resolution, e.g., 30 arc-seconds for the Pacific Northwest (Rogers 2011). For 30-arc-second grid cells, the chance that a fire event spreads throughout an entire grid cell is much higher. In this case, part_burn may be defined as the percentage of total available fuel burned within the fireline, rather than the area touched by the fireline. Given that the resolution used in the present project (5 arc-minutes) is intermediate between the 30-arc-second resolution and the 0.5° resolution, we calculated FRI by using the alternate interpretation (i.e., for any year, a grid cell with a part_burn value greater than zero was considered to have burned 100 percent of that cell). MC1 generally simulated many years with very small part_burn values. Therefore, when we used the alternative interpretation, the resulting FRI values were generally smaller and had poorer correspondence with values reported by Leenhouts (1998).

MC1 uses two parameters to control fire occurrence: fine fuel moisture code (FFMC) and build-up index (BUI). FFMC and BUI thresholds are defined for each of eight broad physiognomic categories. These 16 thresholds are difficult to parameterize when simulating broad regions with diverse vegetation types and fire regimes. Optimizing parameters for one region resulted in degrading model performance in another. For example, when the fire occurrence parameters were set to maximize correspondence of grassland in the eastern Great Plains with those published by Küchler (1964), the model also forecast large areas of grassland in New England. Optimizing the fire parameters is possible when a small area is being simulated. For example, King et al. (2013) were able to significantly improve MC1 simulation of the fire regime at Wind Cave National Park by adjusting fire occurrence parameters and making a few small alterations to the model code. It is unclear, however, whether the various fire regimes of a continent can be sufficiently calibrated by using only 16 parameters representing just eight physiognomic types.

The correlation between MC1 estimates of streamflow and gage measurements is not necessarily a good indication of model skill because both MC1 and the stream gages were responding to precipitation, and some correlation was to be expected. MC1, however, was not designed to be a hydrology model, and its hydrologic algorithms are relatively simplistic. It operates at a monthly time-step, which is coarse relative to most hydrology models. It does not simulate unsaturated flow through soil and instead uses a simple "bucket model," where each soil layer needs to be saturated before any water moves to the next layer below. Determination of the water-holding capacity for each layer is based on the soil texture and organic matter fraction calculated by the model. MC1 does not simulate routing of water through the watershed. Streamflow is calculated by simply summing streamflow values of individual grid cells within the drainage basin. Snow accumulation and melt are modeled as simple linear functions of temperature thresholds.

In other words, MC1's ability to approximate streamflow reported by gages is dependent on MC1's simulation of evapotranspiration (ET). We believe that the simplistic nature of MC1's hydrologic algorithms is somewhat mitigated by MC1's coarse time step. Therefore, when MC1 overestimates streamflow, we generally interpret it to mean that MC1 is underestimating ET in the basin. Conversely, when MC1 underestimates streamflow, we interpret it to mean that MC1 is overestimating ET in the basin. As was the case when we compared simulated carbon stocks with the NBCD2000 (Kellindorfer et al. 2012), comparing MC1 streamflow values with gage values is complicated by the fact that MC1 simulates ET driven by PNV, not actual vegetation.

Although the MC1 hydrology is relatively simple and functions at a coarse time resolution, under some circumstances there can potentially be some advantages to using these data. MC1 does provide an indication of future hydrology patterns under a changing vegetation cover, which is something that some more sophisticated hydrology models do not provide. MC1 does provide hydrology data in synchrony with other time-varying ecosystem variables, such as carbon pools and fire. Also, it might be argued that, when looking at hydrology patterns for the mid 21st century onward, a monthly time-step is probably about as good a resolution as can be reasonably simulated, given the large uncertainty in the magnitude, timing, and intensity of future precipitation.

MC1 belongs to a class of models called dynamic global vegetation models (DGVMs). DGVMs were initially designed to study large-scale (continental to global) impacts of climate and land-use change on ecosystems of the world (Neilson and Running 1996). Early DGVMs generally were run at relatively coarse grids. For example, simulations of the conterminous United States for VEMAP model comparisons were done by using 0.5° resolution (Kittel et al. 2004). As simulations were run at smaller grid cell sizes, additional ecosystem processes not included in the original model have become more significant. Already mentioned are reinterpretations of the part_burn output variable and lack of cell-to-cell routing of water. Cell-to-cell spread of fire can also be significant at the smaller grid cell sizes. Currently, when MC1 simulates the occurrence of fires, they tend to happen over contiguous patches of cells because of autocorrelation of the weather data. When simulating an area by using small grid cells, it would be preferred to simulate fire spread between cells, where a cell not suitable for initial ignition is ignited through fire spread dynamics. Because MC1 simulates many thousands of grid cells and the model code is structured to run optimally on parallel processors, modifying MC1 code to simulate cell-to-cell interaction is a difficult task. It would require overhauling the overall framework of code execution.

MC1 code and algorithms are continually updated by an active community of users. Because of the simulations performed for this report, multiple code updates and improvements have been made. A key improvement, in particular, is that MC1 has been rewritten in C++, primarily for improved computational efficiency. The new version is called MC2. All versions of the code can be obtained at the MC1 DGVM users website (https://sites.google.com/site/mc1dgvmusers/). Further, new applications of MC1 and MC2 using new climate input datasets and new calibrations are ongoing. The results of those simulations should be considered for use in research and assessments.

Acknowledgments

We thank James Strittholt and the Conservation Biology Institute (CBI). Much of the early work for this project was conducted at the CBI Corvallis office under a collaboration agreement. We thank Dominique Bachelet (CBI) for her generous and collegial discussions and review of an early draft of the manuscript. We thank Ken Ferschweiller (CBI) for his assistance with MC1 code and downscaling scripts. We also thank David King (CBI) for informative discussions on simulating biogeography and fires with dynamic global vegetation models. Computing facilities and support for John B. Kim was provided by the USDA Forest Service Pacific Northwest Research Station and the Western Wildlands Environmental Threat Assessment Center.

English Equivalents

1 millimeter (mm) = 0.0394 inch
1 meter (m) = 3.28 feet
1 kilometer (km) = 0.621 mile
1 square meter (m^2) = 10.76 square feet
1 square kilometer (km^2) = 0.386 square mile
1 cubic meter (m^3) = 35.3 cubic feet
1 gram (g) = 0.0352 ounce
1 teragram (tg) = 2.205 x 10^9 pounds
1 petagram (pg) = 2.205 x 10^{12} pounds
1 pascal = 1.45 x 10^{-4} pounds per square inch
1 kilopascal (kpa) = 0.145 pounds per square inch
(1.8 × °C) + 32 = °F

References

Anderson, M.K. 1990. The historic role of fire in the North American grassland. In: Collins, S.L.; Wallace, L.L., eds. Fire in the North American tallgrass prairies. Norman, OK: University of Oklahoma Press: 8–18.

Barr, B.R.; Koopman, M.E.; Deacon Williams, C.; Bynne, S.J.; Hamilton, R.; Doppelt, B. 2010. Preparing for climate change in the Klamath Basin. Eugene, OR: University of Oregon, National Center for Conservation Science & Policy and the Climate Leadership Initiative. 36 p.

Bachelet, D.; Lenihan, J.M.; Daly, C.; Neilson, R.P.; Ojima, D.S.; Parton, W.J. 2001a. MC1: a dynamic vegetation model for estimating the distribution of vegetation and associated ecosystem fluxes of carbon, nutrients, and water. Gen. Tech. Rep. PNW-GTR-508. Portland, OR: U.S. Department of Agriculture, Forest Service, Pacific Northwest Research Station. 95 p.

Bachelet, D.; Neilson, R.P.; Lenihan, J.M.; Drapek, R.J. 2001b. Climate change effects on vegetation distribution and carbon budget in the United States. Ecosystems. 4: 164–185.

Bachelet, D.; Neilson, R.P.; Lenihan, J.M.; Drapek, R.J. 2004. Regional differences in the carbon source-sink potential of natural vegetation in the U.S.A. Environmental Management. 33 Supplement: S23–S43.

Bachelet, D.; Lenihan, J.M.; Neilson, R.P.; Drapek, R.; Kittel, T. 2005. Simulating the response of natural ecosystems and their fire regimes to climate variability in Alaska. Canadian Journal of Forest Research. 35(9): 2244–2257.

Bachelet, D.; Lenihan, J.; Neilson, R. 2007. The importance of climate change for future wildfire scenarios in the western United States. In: Ebi, K.L.; Meehl, G.A.; Bachelet, D.; Twilley, R.R.; Boesch, D.F., eds. Regional impacts of climate change: four case studies in the United States. Arlington, VA: Pew Center on Global Climate Change: 22–41.

Briggs, J.M.; Knapp, A.K.; Brock, B.L. 2002. Expansion of woody plants in tallgrass prairie: a fifteen-year study of fire and fire-grazing interactions. American Midland Naturalist. 147(2): 287–294.

Chiarucci, A.; Araujol, M.B.; Decocq, G.; Beierkhhnlein, C.; Fernandex-Palacios, J.M. 2010. The concept of potential natural vegetation: an epitaph? Journal of Vegetation Science. 21: 1172–1178.

Cohen, J. 1960. A coefficient of agreement for nominal scales. Educational and Psychological Measurement. 41: 687–699.

Daly, C. 2006. Guidelines for assessing the suitability of spatial climate datasets. International Journal of Climatology. 26: 707–721.

Daly, C.; Bachelet, D.; Lenihan, J.M.; Neilson, R.P.; Parton, W.; Ojima, D. 2000. Dynamic simulations of tree-grass interactions for global change studies. Ecological Applications. 10(2): 449–469.

Daly, C.; Gibson, W.P.; Taylor, G.H.; Johnson, G.L.; Pasteris, P. 2002. A knowledge-based approach to the statistical mapping of climate. Climate Research. 22: 99–113.

Daly, C.; Halbleib, M.; Smith, J.I.; Gibson, W.P.; Doggett, M.K.; Taylor, G.H.; Curtis, J.; Pasteris, P.P. 2008. Physiographically sensitive mapping of climatological temperature and precipitation across the conterminous United States. International Journal of Climatology. 28: 2031–2064.

Daly, C.; Neilson, R.P.; Phillips, D.R. 1994. A statistical-topographic model for mapping climatological precipitation over mountainous terrain. Journal of Applied Meteorology. 33(2): 140–158.

Doppelt, B.; Hamilton, R.; Deacon Williams, C.; Koopman, M. 2008. Preparing for climate change in the Rogue River basin of southwest Oregon: stressors, risks, and recommendations for increasing resilience and resistance in human, built, economic, and natural systems. Eugene OR: University of Oregon. 39 p.

Esri. 2009. ArcMap 9.2. Redlands, CA: Esri, Inc.

Esri. 2010. ArcMap 10.0. Redlands, CA: Esri, Inc.

Fowler, H.J.; Blenkinsop, S.; Tebaldi, C. 2007. Linking climate change modeling to impacts studies: recent advances in downscaling techniques for hydrological modeling. International Journal of Climatology. 27: 1547–1578.

Galbraith, H.; Smith, J.B.; Jones, R. 2006. Biodiversity changes and adaptation. In: Smith, J.B.; Mendelsohn, R., eds. The impact of climate change on regional systems: a comprehensive analysis in California. Northampton, MA: Edward Elgar Publishing, Inc.: 86–99.

Gonzalez, P.; Neilson, R.P.; Lenihan, J.M.; Drapek, R.J. 2010. Global patterns in the vulnerability of ecosystems to vegetation shifts due to climate change. Global Ecology and Biogeography. 19(6): 755–768.

Gordon, H.; O'Farrell, S.; Collier, M.; Dix, M.; Totstayn, L.; Kowalczyk, E.; Hirst, T.; Watterson, I. 2010. The CSIRO Mk3.5 climate model. CAWCR Tech. Rep. No. 021. Melbourne, Victoria, Australia: Centre for Australian Weather and Climate Research. 62 p.

Gucinski, H. 2005. Terrestrial and aquatic natural ecosystems: potential responses to global climate change. In: Joyce, L.; Haynes, R.; White, R.; Barbour, J., tech. coords. Bringing climate change into natural resources management: proceedings of a workshop. Gen. Tech. Rep. PNW-GTR-706. Portland, OR: U.S. Department of Agriculture, Forest Service, Pacific Northwest Research Station: 41–66.

Halofsky, J.E.; Hemstrom, M.A.; Conklin, D.R.; Halofsky, J.S.; Kerns, B.K.; Bachelet, D. 2013. Assessing potential climate change effects on vegetation using a linked model approach. Ecological Modeling. 266: 131–143.

Halofsky, J.E.; Peterson, D.L.; Aubry, C.; Dowling, C.; Acker, S. 2011. Climate change and vegetation management at Olympic National Forest and Olympic National Park. In: Halofsky, J.E.; Peterson, D.L.; O'Halloran, K.A.; Hawkins, C., eds. Adapting to climate change at Olympic National Forest and Olympic National Park. Gen. Tech. Rep. PNW-GTR-844. Portland, OR: U.S. Department of Agriculture, Forest Service, Pacific Northwest Research Station: 61–90. Chapter 6.

Hasumi, H.; Emori, S. 2004. K-1 coupled GCM (MIROC) description. K-1 Tech. Rep. 1. Tokyo, Japan: Center for Climate System Research. 34 p.

International Panel of Climate Change Working Group II [IPCC WGII]. 2014. Climate change 2014: impacts, adaptation, and vulnerability. working group II contribution to the IPCC 5th assessment report—changes to the underlying scientific/technical assessment. http://ipcc-wg2.gov/AR5/report/final-drafts/. (2 May 2014).

Johns, T.C.; Gregory, J.M.; Ingram, W.J.; Johnson, C.E.; Jones, A.; Lowe, J.A.; Mitchell, J.F.B.; Roberts, D.L.; Sexton, D.M.H.; Stevensons, D.S.; Tett, S.F.B.; Woodage, J.J. 2003. Anthropogenic climate change for 1860 to 2100 simulated with the HadCM3 model under updated emissions scenarios. Climate Dynamics. 20(6): 583–612.

Kellindorfer, J.; Walker, W.; LaPoint, E.; Bishop, J.; Cormier, T.; Fiske, G.; Hoppus, M.; Kirsch, K.; Westfall, J. 2012. NACP aboveground biomass and carbon baseline data (NBCD 2000), U.S.A., 2000. [Dataset]. http://dx.doi.org/10.3334/ORNLDAAC/1081. (15 July 2014).

Kern, J.S. 1995. Geographic patterns of soil water-holding capacity in the contiguous USA. Soil Science Society of America Journal. 59: 1126–1133.

Kerns, **B.K.; Hemstrom, M.; Conklin, D.; Yospin, G.; Johnson, B.; Brigham S. 2012.** Approaches to incorporating climate change effects in state and transition simulation models of vegetation. In: Kerns, B.K.; Shlisky, A.J.; Daniel, C.J., tech. eds. The first state-and-transition landscape simulation modeling conference proceedings. Gen. Tech. Rep. PNW-GTR-869. Portland, OR: U.S. Department of Agriculture, Forest Service, Pacific Northwest Research Station: 161–171.

King, D.A.; Bachelet, D.M.; Symstad, A.J. 2013. Vegetation projections for Wind Cave National Park with three future climate scenarios. Nat. Res. Tech. Rep. NPS/WICA/NRTR-2013/681. Fort Collins, CO: U.S. Department of the Interior, National Park Service. 57 p.

Kittel, T.G.F.; Rosenbloom, N.A.; Royle, J.A.; Daly, C.; Gibson, W.P.; Fisher, H.H.; Thornton, P.; Yates, D.N.; Aulenbach, S.; Kaufman, C.; McKeown, R.; Bachelet, D.; Schimel, D.S. 2004. VEMAP phase 2 bioclimatic database. I. Gridded historical (20th century) climate for modeling ecosystem dynamics across the conterminous USA. Climate Research. 27: 151–170.

Koopman, D.S.; Nauman, R.S.; Leonard, J.L. 2010. Projected future climate and ecological conditions in San Luis Obispo County. Ashland, OR: National Center for Conservation Science & Policy. 33 p.

Kueppers, L.; Riley, W.; Jin, J., Subin, Z.; Torn, M. 2009. Ecosystem feedbacks to climate change in California: integrated climate forcing from vegetation redistribution. Final project report CEC-500-2009-075. Sacramento, CA: California Energy Commission, Public Interest Energy Research Program.

Küchler, A.W. 1964. Potential natural vegetation of the conterminous United States. [Map]. Spec. Pub. No. 36. New York: American Geographical Society.

Landis, J.R.; Koch, G.G. 1977. The measurement of observer agreement for categorical data. Biometrics. 33: 159–174.

Leenhouts, B. 1998. Assessment of biomass burning in the conterminous United States. Conservation Ecology. 2(1): 1. http://www.consecol.org/vol2/iss1/art1/. (15 July 2014).

Lenihan, J.M.; Bachelet, D.; Neilson, R.P.; Drapek, R. 2008. Simulated response of conterminous United States ecosystems to climate change at different levels of fire suppression, CO_2 emission rate, and growth response to CO_2. Global and Planetary Change. 64 (1–2): 16–25.

Lenihan, J.M.; Daly, C.; Bachelet, D.; Neilson, R.P. 1998. Simulating broad-scale fire severity in a dynamic global vegetation model. Northwest Science. 72: 91–103.

Lenihan, J.M.; Drapek, R.; Bachelet, D.; Neilson, R.P. 2003. Climate change effects on vegetation distribution, carbon stocks, and fire regimes in California. Ecological Applications. 13: 1667–1681.

Lenihan, J.M.; Drapek, R.; Neilson, R. 2006. Terrestrial ecosystem changes. In: Smith, J.B.; Mendelsohn, R., eds. The impact of climate change on regional systems: a comprehensive analysis of California. Northampton, MA: Edward Elgar Publishing, Inc.: 60–85.

Lett, M.S.; Knapp, A.K. 2005. Woody plant encroachment and removal in mesic grassland: production and composition responses of herbaceous vegetation. The American Midland Naturalist. 153(2): 217–231.

MacDonald, K.B.; Kloosterman, B. 1984. The Canada Soil Information System (CanSIS) general user's manual. Contribution No. 83-59-E. Ottawa, ON: Agriculture Canada, Research Branch, Land Resources Research Institute. 92 p.

McKenney, D.W.; Hutchinson, M.F.; Papadopol, P.; Price, D.T. 2004. Evaluation of alternative spatial models of vapour pressure in Canada. In: Proceedings American Meteorological Society 26th conference on agricultural and forest meteorology. [CD-ROM]. 11 p.

McLachlan, M.; Bartuszevige, A.; Pool, D. 2011. Evaluating the potential of the conservation reserve program to offset projected impacts of climate change on the lesser prairie chicken (*Tympanuchus pallidicinctus*). Washingon, DC: U.S. Department of Agriculture, Natural Resources Conservation Service. 44 p.

Mitchell, T.D.; Carter, T.R.; Jones, P.D.; Hulme, M.; New, M. 2004. A comprehensive set of high-resolution grids of monthly climate for Europe and the globe: the observed record (1901–2000) and 16 scenarios (2001–2100). Working paper 55. Norwich, United Kingdom: Tyndall Centre for Climate Change Research. 30 p.

Moss, R.H.; Edmonds, J.A.; Hibbard, K.A.; Manning, M.R.; Rose, S.K.; Van Vuuren, D.P.; Carter, T.R.; Emori, S.; Kainuma, M.; Kram, T.; Meehl, G.A.; Mitchell, J.F.B.; Nakicenovic, N.; Riahi, K.; Smith, S.J.; Stouffer, R.J.; Thomson, A.M.; Weyant, J.P.; Wilbanks, T.J. 2010. The next generation of scenarios for climate change research and assessment. Nature. 463(7282): 747–756.

Nachtergaele, F.; van Velthuizen, H.; Vereist, L. 2009. Harmonized world soil database: version 1.1 [data documentation]. Rome, Italy, and Laxenburg, Austria: Food and Agriculture Organization of the United Nations (FAO), International Institute for Applied Systems Analysis (IIASA), ISRIC—World Soil Information; Institute of Soil Science—Chinese Academy of Sciences (ISSCAS), Joint Research Centre of the European Commission (JRC).

Nakicenovic, N.; Alcamo, J.; Davis, G.; de Vries, B.; Fenhann, J.; Gaffin, S.; Gregory, K.; Grübler, A.; Jung, T.Y.; Kram, T.; Lebre La Rovere, E.; Michaelis, L.; Mori, S.; Morita, T.; Pepper, W.; Pitcher, H.; Price, L.; Riahi, K.; Roehrl, A.; Rogner, H.; Sankovski, A.; Schlesinger, M.; Shukla, P.; Smith, S.; Swart, R.; van Rooijen, S.; Victor, N.; Dadi, Z. 2000. Emissions scenarios: a special report of working group III of the Intergovernmental Panel on Climate Change. New York: Cambridge University Press. 20 p.

U.S. Department of Agriculture, Natural Resources Conservation Service [USDA NRCS]. 1979. Exploratory soil survey of Alaska; STATSGO Publication. 1:1,000,000 scale. Fort Worth, TX.

U.S. Department of Agriculture, Natural Resources Conservation Service [USDA NRCS]. 1994. State soil geographic (STATSGO) data base for the conterminous United States. Misc. Publ. 1492. Lincoln, NE. http://water.usgs.gov/GIS/metadata/usgswrd/XML/ussoils.xml. (16 July 2014).

Neilson, R.P. 1995. A model for predicting continental-scale vegetation distribution and water balance. Ecological Applications. 5: 362–385.

Neilson, R.P.; Running, S.W. 1996. Global dynamic vegetation modeling: coupling biogeochemistry with biogeography models. In: Walker, B.; Steffen, W., eds. Global change and terrestrial ecosystems Cambridge, United Kingdom: Cambridge University Press: 451–465.

New, M.; Hulme, M.; Jones, P.D. 2000. Representing twentieth century space-time climate variability. Part 2: Development of 1901–96 monthly grids of terrestrial surface climate. Journal of Climate. 13: 2217–2238.

Parton, W.J.; Schimel, D.S.; Cole, C.V.; Ojima, D.S. 1987. Analysis of factors controlling soil organic matter levels in Great Plains grasslands. Soil Science Society of America Journal. 51: 1173–1179.

Price, D.T.; McKenney, D.W.; Papadopol, P.; Logan, T.; Hutchinson M.F. 2004. High resolution future scenario climate data for North America. In: Proceedings of the American Meteorological Society 26th conference on agriculture and forest meteorology. [CD-ROM]. 13 p. http://ams.confex.com/ams/pdfpapers/78202.pdf. (16 July 2014).

Riahi, K.; Rao, S.; Krey, V.; Cho, C.; Chirkov, V.; Fischer, G.; Kindermann, G.; Nakicenovic, N.; Rafaj, P. 2011. RCP 8.5—a scenario of comparatively high greenhouse gas emissions. Climatic Change. 109(1–2): 33–57.

Rieger, S.; Schoephorster, D.B.; Furbush, C.E. 1979. Exploratory soil survey of Alaska. Fort Worth, TX: U.S. Department of Agriculture, Natural Resources Conservation Service. 213 p.

Rogelj, J.; Meinshausen, M.; Knutti, R. 2012. Global warming under old and new scenarios using IPCC climate sensitivity range estimates. Nature Climate Change. 2(4): 248–253.

Rogers, B.M.; Neilson, R.P.; Drapek, R.; Lenihan, J.M.; Wells, J.R.; Bachelet; D.; Law, B.E. 2011. Impacts of climate change on fire regimes and carbon stocks of the Pacific Northwest. Journal of Geophysical Research. 116, G03037, doi:10.1029/2011JG001695.

Schwarz, R.E.; Alexander, R.B. 1995. State soil geographic (STATSGO) data base for the conterminous United States. Reston, VA: U.S. Department of the Interior, Geological Survey. http://water.usgs.gov/GIS/metadata/usgswrd/XML/ussoils.xml. (14 July 2014).

Schimel; VEMAP2 Participants. 2004. VEMAP phase 2 bioclimatic database. I. Gridded historical (20^{th} century) climate for modeling ecosystem dynamics across the conterminous USA. Climate Research. 27: 151–170.

Somodi, I.; Molnar, Z.; Evald, J. 2012. Towards a more transparent use of the potential natural vegetation concept—and answer to Chiarucci et al. Journal of Vegetation Science. 23(3): 590–595.

Van Vuuren, D.P.; Edmonds, J.; Kainuma, M.; Riahi, K.; Thomson, A.; Hibbard, K.; Hurtt, G.C.; Kram, T.; Krey, V.; Lamarque, J.; Masui, T.; Meinshausen, M.; Nakicenovic, N. 2011. The representative concentration pathways: an overview. Climatic Change. 109: 5–31.

Waring, R.H.; Running, S.W. 1998. Forest ecosystems: analysis at multiple scales. 2^{nd} ed. Burlington, MA: Elsevier Academic Press. 370 p.

Appendix 1: Description of the Data Files

All data are in latitudes and longitudes. Grids consist of 720 rows by 1,392 columns. Each grid cell is 5 arc-minutes in width and in latitude and longitude, which corresponds to about 8 km at mid-latitude. The bounding coordinates of the rectangular simulated area are 85.0 to 25.0 latitude, -52.0 to -168.0 in longitude. Datum for the dataset is the North American Datum of 1983 (NAD83).

Data are stored in NetCDF format. NetCDF (Network Common Data Form) is a set of interfaces for array-oriented data access and a freely distributed collection of data access libraries for C, Fortran, C++, Java, and other languages. The NetCDF libraries support a machine-independent format for representing scientific data. Together, the interfaces, libraries, and format support the creation, access, and sharing of scientific data. Our reasons for using NetCDF include (1) it is good at handling multiple variables and multiple dimensions; (2) NetCDF files are self-describing and portable; (3) NetCDF files are accessible multiple ways including the access libraries mentioned above and ArcMap tools. For more information on NetCDF, see http://www.unidata.ucar.edu/software/netcdf/#documentation.

Climate files are organized so that the data are in three-dimensional matrices: time × latitude × longitude. The unit of the time dimension is 1 month. The soil data file is organized so that the data are in a three-dimensional matrix, band × latitude × longitude, where the band dimension consists of 10 soil attributes: mineral_depth (mm), sand[surface] (percentage), sand[intermediate] (percentage), sand[deep] (percentage), clay[surface] (percentage), clay[intermediate] (percentage), clay[deep] (percentage), rock_fragment_mineral[surface] (percentage), rock_fragment_mineral[intermediate] (percentage), and rock_fragment_mineral[deep] (percentage). The three depths correspond to surface 0 to 50 cm, intermediate 50 to 150 cm, and deep ≥ 150 cm. MC1 output variables are also available as three-dimensional matrices, time × latitude × longitude, where the unit of the time dimension is a year.

Appendix 2: Obtaining Copies of the Data

Input and output data files can be obtained from an anonymous ftp site: ftp://gcc.fsl.orst.edu/MC1/8K_Version_165_MC1_2012_Climate/. There are two subdirectories “Inputs” and “Outputs.” “Inputs” includes all the climate data files for all scenarios and “Outputs” includes all variables coming out of the MC1 model. All files are in NetCDF format and are compliant with the climate and forecast (CF) metadata convention standards. Additional metadata files in the Extensible Markup Language (XML) will be included to correspond with each NetCDF file and these will conform to the Content Standard for Digital Geospatial Metadata (CSDGM) standards. Documentation for NetCDF can be found at http://www.unidata.ucar.edu/software/netcdf/docs/. Utilities for reading NetCDF files can be found at http://nco.sourceforge.net/ and at http://www.unidata.ucar.edu/software/netcdf/fan_utils.html.

Inputs

Under the “Inputs” directory are directories for all nine future climate projections as well as one for historical climate data. In each of these are separate files for each of the climate variables: ppt (precipitation), Tmax (average of daily maximum two meter temperatures per month), Tmin (average of daily minimum two meter temperatures per month), tmp (average temperature at two meters above land surface), and vpr (average monthly surface vapor pressure).

Outputs

MC1 can potentially output more than 900 annual or monthly variables, but only 25 annual variables are included. Under the “Outputs” directory are subdirectories for all of the different output variable types. The variable types and numbers of variables saved include biogeography (two variables), fire (two variables), leaf_area_index (two variables), carbon_stock (twelve variables), carbon_fluxes (four variables), and hydrology (three variables). Within each variable-type there are two files for each future climate projection, with and without fire suppression. For example, under the carbon_fluxes directory for the CSIRO A1B projection there are two files: csiro_a1b_c_fluxes.nc (for the fire-suppression run) and csiro_a1b_nfs_c_fluxes.nc (for the no-fire-suppression run).

Glossary

AGVeg—Aboveground vegetation carbon simulated by MC1.

ANUSPLIN—A package of programs often used to created gridded climate maps from weather station data. ANUSPLIN uses a thin plate spline surface fitting technique.

CRU—Climatic Research Unit. Our source for gridded historical global climate at a half-degree resolution.

CSIRO—The Commonwealth Scientific and Industrial Research Organization is Australia's national science agency. The Mk 3.5 climate model developed at CSIRO is a source for future climate scenarios.

GCM—General circulation models.

GHG—Greenhouse gas.

HadCM3—Hadley Centre Coupled Model, version 3. A climate model that is a source for future climate scenarios.

huss—Surface specific humidity.

IPCC—Intergovernmental Panel on Climate Change.

HWSD – Harmonized World Soil Database.

MIROC—The Center for Climate System Research at the University of Tokyo. The MIROC 3.2 medres model is one of our sources for future climate scenarios.

NBCD2000—National Biomass and Carbon Dataset for the year 2000.

NetCDF—Network Common Data Form. NetCDF is a set of software libraries and self-describing, machine-independent data formats that support the creation, access, and sharing of array-oriented scientific data.

NAD83—North American Datum of 1983.

PP—A proprietary file format for meteorological data developed by the Met Office, the United Kingdom's national weather service.

ppt—Monthly sum precipitation.

PRISM—Parameter-Elevation Regressions on Independent Slopes Model. A climate mapping system and our source for high-spatial-resolution (relative to CRU) gridded historical climate within the United States and parts of Canada.

ps—Surface air pressure.

SRES—Special Report on Emissions Scenarios. Published by the IPCC. This contained a set of greenhouse gas emission scenarios.

Tmax—Monthly mean of daily maximum temperatures.

Tmean—Mean monthly temperature.

Tmin—Monthly mean of daily minimum temperatures.

vpr—Vapor pressure.

Pacific Northwest Research Station

Web site	http://www.fs.fed.us/pnw
Telephone	(503) 808-2592
Publication requests	(503) 808-2138
FAX	(503) 808-2130
E-mail	pnw_pnwpubs@fs.fed.us
Mailing address	Publications Distribution Pacific Northwest Research Station P.O. Box 3890 Portland, OR 97208-3890

Federal Recycling Program
Printed on Recycled Paper

U.S. Department of Agriculture
Pacific Northwest Research Station
1220 SW 3rd Ave., Suite 1400
P.O. Box 3890
Portland, OR 97208-3890